Norwegian University
of Life Sciences

Master's Thesis 2021   30 ECTS
Faculty of Science and Technology

Exploring the Effect of Ionic Diffusion on Extracellular Potentials in the Brain

Christine Brinchmann
MSc. Environmental Physics and Renewable Energy

Acknowledgements

This thesis marks the end of my Master's degree at the Norwegian University of Life Sciences (NMBU) and the end of 5 years of studies at NMBU. I am grateful for everything I have learned and the paths it has opened for me.

Thanks to my supervisor Geir Halnes for always answering my questions and especially for our weekly meetings. I appreciate all the help and the valuable feedback I got throughout the semester. I would also like to thank Gaute Einevoll for introducing me to the field of neuroscience.

Finally, I would like to thank my friends and family for their support.

Ås, June 1, 2021

_____

Christine Brinchmann

Abstract

Ionic concentration gradients can exist in the extracellular space (ECS) due to neuronal activity that can change the local ionic composition. Diffusion and electrical drift are two processes that move ions around in the extracellular space. These processes can be described by the Nernst-Planck equation. Ions diffuse along concentration gradients. Since ions carry charge, this process can give rise to electric currents, which, in turn, can result in a diffusion potential.

The question under investigation is if diffusion potentials in ECS are large enough to affect the measurements of local field potentials (LFPs) in the brain? Diffusion potentials are slow-changing potentials, so its possible contributions to the LFPs would be for low frequencies [1]. To explore the effect of diffusion potentials, I compared power spectrum densities (PSDs) of diffusion potentials to PSDs of LFPs recordings.

I estimated the diffusion potentials from extracellular concentration data collected from various articles. The concentration data were obtained from different experiments. Instead of numerically simulating how the diffusion potential changed, I approximated the diffusion potential by an exponentially decaying function. For more realistic estimates, I used time constants from temporal concentration data. Then, I estimated the PSDs of the diffusion potentials from each data set.

For LFP data, I found and used data files with LFP recordings. For these data files, I calculated average PSDs. In addition, I collected LFP data represented as PSDs from figures in articles,

At low frequencies (< 1 Hz), I found that PSD of the highest diffusion potentials had similar powers as the lowest PSDs of LFP measurements. Therefore, there may be a slight possibility that diffusion potentials can contribute to the LFP at the lowest frequencies.

I also estimated diffusion potentials at pathological conditions, such as

spreading depression (SD), where concentration gradients are extremely large. I used the same approach and found that the diffusion potentials in these cases could be up to 10 times larger. The PSDs of the pathological diffusion potentials had similar powers as the LFP recordings.

Contents

Chapter 1

Introduction

Isn't it weird how we humans have discovered our brain? Or is it the other way around, how the brain has discovered itself? Today, the eagerness to find out more about the human brain can be found in the field of neuroscience. Neuroscience is the study of the brain and the nervous system. The nervous system in vertebrates is divided into the peripheral nervous system (PNS) and the central nervous system (CNS) [2]. The PNS is the part that connects the nerve cells throughout our body with the nerve cells in the CNS (the brain and the spinal cord) [2]. The building blocks of the nervous system are nerve cells (also called neurons) and glial cells. Both cells have varying membrane potentials but only neurons produce action potentials, which are important for the electric information signaling in the brain.

The branched structure of neurons makes them different from cells in other tissue. The standard neuron consists of the soma (cell body), dendrites, and an axon. Neurons connect to thousands of other neurons, and they form large networks in the brain. A neuron receives input from other neurons through synapses at its dendrites, and the information moves towards the soma. If the input is strong enough or numerous enough, the neuron produces an action potential and propagates it along the axon. At the axon terminals, the neuron connects to other neurons' dendrites through synapses, and the information can be forwarded to other parts of the network.

Neurons have a different distribution of ion species between the inside (intracellular) and outside (extracellular). When the neurons are resting, they are polarized, meaning that they have a potential difference over the membrane. The neuron uses this concentration difference to generate action potentials: sodium ions (Na^+) flow into the neuron, followed by an efflux of

potassium ions (K^+) through the selective opening and closing of ion channels in the membrane. Concentration changes, on the inside and the outside, due to a single action potential are negligible.

The space between the cells in neural tissue is called the extracellular space (ECS). The ECS contains a conductive saline solution and accounts for about 20 % of the tissue volume in the brain (volume fraction $\alpha \sim 0.20$) [3]. The volume fraction of ECS can vary across different brain regions, and for various conditions, for example, it differs during sleep and waking hours.

During periods with prolonged and intense neuron firing, concentration changes in ECS can become significant over time. Such concentration changes in the ECS can affect the firing pattern of neurons [4]. Other effects, which are more important for this project, is that concentration gradients in the ECS can give rise to diffusion potentials. Electrical potentials in the ECS are often measured to obtain information about the underlying neural activity. But, is everything measured due to neuronal activity, or can other effects in the ECS be visible in the measurements?

During periods with prolonged and intense neuron firing, concentration changes in ECS can become significant over time. Such concentration changes in the ECS can affect the firing pattern of neurons [4]. Other effects, which are more important for this project, is that concentration gradients in the ECS can give rise to diffusion potentials. Electrical potentials in the ECS are often measured to obtain information about the underlying neural activity. But, is everything measured due to neuronal activity, or can other effects in the ECS be visible in the measurements?

There are many previous recordings of extracellular potentials. Local field potential (LFP) is the low-frequency part of the extracellular potential and is measured because it can tell us what neurons do. The main assumption when recording LFP is that it only reflects neuronal activity. However, if there exist concentration gradients in the ECS, there might also occur diffusion potentials. So the questions are: Are diffusion potentials large enough to affect LFP recordings in the ECS? Do the diffusion potential change fast enough to be a meaningful part of the ECS potential recordings? The second question is included because many LFP measurements have a cutoff frequency of about 1 Hz, which means that very slow varying potentials will be filtered out.

Halnes et al. [1] found through simulation of 10 pyramidal neurons, with and without diffusion in ECS, that diffusion played a role in the slow

timescale. They concluded that diffusion may play a role and contribute to the lower frequencies of the potential. Since this was a simulation, the conclusions only apply to the stimulated system. Therefore, it motivates for a follow-up study based on experimental data.

The objective of my project is to see if diffusion potentials in ECS can contribute to the recorded extracellular potentials. Does the assumption stating that diffusion potentials can be neglected apply to all cases? To do so, I collected ionic concentration data in ECS from published articles. Then I estimated diffusion potentials and their exponential decay through time. Using this time series for the diffusion potentials, I calculated the power spectrum densities (PSDs) to make comparisons easier. I also collected LFP data from a database and PSD of LFP data from published articles. The PSDs of diffusion potentials were compared to these PSDs of LFP recordings. The questions become: Will the PSDs overlap? Or will the PSDs of LFP recordings have higher power than the PSDs of diffusion potentials for the entire frequency range?

This thesis is divided into five chapters. You are now on the last paragraph of the introduction chapter. Later in the method chapter, I describe the project approach and present the assumptions. After that comes a presentation of the results, followed by a discussion and conclusion chapter. The next chapter contains the background theory relevant to this thesis. Enjoy!

Chapter 2

Background

2.1 The Nernst-Planck equation

Diffusion is the movement of ions due to concentration gradients. Ions diffuse with a flux toward places with lower concentrations. The diffusion flux depends on the diffusion constant of an ion species and the concentration gradient present. To find the diffusion flux of an ion species k, $\boldsymbol{J}_{\mathrm{diff},k}$, we can use Fick's law:

$$\boldsymbol{J}_{\mathrm{diff},k} = -D_k^* \nabla c_k, \tag{2.1}$$

where D_k^* is the diffusion coefficient and ∇c_k is the concentration gradient to ion species k. The diffusion coefficient is a material property and its value for an ion species k depends on the material the ions diffuses in. We obtain a high diffusion flux for ions with large diffusion constants or large concentration gradients. A large diffusion flux means that ions diffuse faster, leveling out the concentration gradient faster.

Ions can also move due to an electric field because of an ion's charge. The charge, positive or negative, decides which direction an ion moves in the electric field. The valency, z_k, (also called the charge number) represents the number of elementary charges to an ion. The field flux of an ion species k, $\boldsymbol{J}_{\mathrm{field},k}$, depends on the potential gradient and can be found by:

$$\boldsymbol{J}_{\mathrm{field},k} = -\frac{D_k^* z_k F}{RT} c_k \nabla \Phi, \tag{2.2}$$

where D_k^* is the diffusion coefficient and z_k is the valence of the ion. c_k is the concentration of ion species k and $\nabla \Phi$ is the potential gradient. F is

Faraday's constant, R is the gas constant and T is the absolute temperature.

There exist table values for diffusion coefficients for different ion species in saline solutions. The extracellular space (ECS) contains such a saline solution, but it has a tortuous structure. Diffusion in ECS is, therefore, prevented by hindrances, such as cell structures and, for example, other molecules in the ECS. These hindrances can be corrected for by introducing a tortuosity factor, λ_n. The diffusion coefficient, D_k^*, in ECS is given by

$$D_k^* = \frac{D_k}{\lambda_n^2}, \tag{2.3}$$

where D_k is the diffusion constant in a saline solution. The value for tortuosity is ~ 1.6 in normal brain tissue [3]. Thus, the diffusion coefficient in ECS is smaller than in dilute solutions, which means that ions diffuse slower in the ECS.

To get an equation for the total flux of an ion species k, we can add the diffusive flux, $\boldsymbol{J}_{\text{diff},k}$, and field flux, $\boldsymbol{J}_{\text{field},k}$, together:

$$\boldsymbol{J}_k = \boldsymbol{J}_{\text{diff},k} + \boldsymbol{J}_{\text{field},k} = -\frac{D_k}{\lambda_n^2}\nabla c_k - \frac{D_k z_k F}{\lambda_n^2 RT}c_k\nabla\Phi. \tag{2.4}$$

This equation is called the Nernst-Planck equation, and it describes the process of electrodiffusion: movements of ion species are affected by both a concentration gradient and a potential gradient. Note that Equation 2.3 is substituted into Equation 2.4.

To describe the relationship between the total flux of an ion species k and the change of that ion's concentration over time, we have the continuity equation:

$$\frac{\partial c_k}{\partial t} = -\nabla \cdot \boldsymbol{J}_k. \tag{2.5}$$

Inserting the total flux, $\boldsymbol{J}_k$, (Equation 2.4) into the continuity equation above, we get:

$$\frac{\partial c_k}{\partial t} = -\frac{D_k}{\lambda_n^2}\nabla^2 c_k + \frac{D_k z_k}{\lambda_n^2 \Psi}\nabla \cdot (c_k\nabla\Phi), \tag{2.6}$$

where $\Psi = RT/F$. This equation is a partial differential equation and is called the time-dependent Nernst-Planck equation. The equation describes the relationship between an ion's concentration change, its concentration gradient, and a potential gradient.

The diffusion flux $\boldsymbol{J}_{\text{diff},k}$, and the field flux, $\boldsymbol{J}_{\text{field},k}$, can be converted into

diffusion current, $\boldsymbol{I}_{\text{diff},k}$, and field current, $\boldsymbol{I}_{\text{field},k}$, by multiplying with $z_k F$:

$$\boldsymbol{I}_{\text{diff},k} = z_k F \boldsymbol{J}_{\text{diff},k} = z_k F \frac{D_k}{\lambda_n^2} \nabla c_k, \tag{2.7}$$

$$\boldsymbol{I}_{\text{field},k} = z_k F \boldsymbol{J}_{\text{field},k} = \frac{D_k z_k^2 F c_k}{\lambda_n^2 \Psi} \nabla \Phi. \tag{2.8}$$

To derive an expression for the total ion current, we must sum the diffusion current and the field current. The total current, including all ions, are then obtained by summing all ion currents:

$$\boldsymbol{I} = \sum_k (\boldsymbol{I}_{\text{diff},k} + \boldsymbol{I}_{\text{field},k}) = -\sum_k z_k F \frac{D_k}{\lambda_n^2} \nabla c_k - \sum_k \frac{D_k z_k^2 F c_k}{\lambda_n^2 \Psi} \nabla \Phi. \tag{2.9}$$

The first term on the right side of Equation 2.9 is the total diffusion current. The second term is the total field current due to an electric field. Assuming that the electric field follows Ohms law, $V = RI$ or $\boldsymbol{J} = \sigma \boldsymbol{E}$, the conductivity σ can be defined as:

$$\sigma = \frac{F}{\Psi} \sum_k \frac{D_k}{\lambda_n^2} z_k^2 c_k. \tag{2.10}$$

2.2 Solution methods

Solving the time-dependent Nernst-Planck equation (Equation 2.6) is challenging. From Equation 2.6, we get a differential equation for each ion species k. In addition, we also need an equation for the potential Φ. There exist two frameworks: the Poisson-Nernst-Planck (PNP) and the electroneutral scheme (also called Kirchhoffs-Nernst-Planck, KNP).

The PNP framework uses Poisson's equation:

$$\nabla^2 \Phi = -\frac{\rho}{\epsilon}, \tag{2.11}$$

where ϵ is the permittivity of the medium (here the ECS), and ρ is charge density [5]. This charge density is equal to the sum from all ion species:

$$\rho = F \sum_k z_k c_k. \tag{2.12}$$

PNP give detailed simulations and physically correct results, but it is ineffi-

cient for numerically solutions [5].

The KNP framework assumes electroneutrality at each point in the system ($\partial c/\partial t = 0$), where there is no neuronal source or sink [5]. If there are no sinks or sources, the net current must be zero. This means that the diffusive and the electric field current must cancel each other out. Inserting the conductivity, σ, (Equation 2.10) into the total current (Equation 2.9) and setting the total current to zero, we get:

$$\sum_k z_k F \frac{D_k}{\lambda_n^2} \nabla c_k = \sigma \nabla \Phi. \tag{2.13}$$

The potential Φ occurs because of concentration gradients (no sources or sinks), such that the diffusion current and field current balance each other. This potential is called the diffusion potential.

2.2.1 Arise of a diffusion potential

Contact between two saline solutions with different concentrations can lead to a diffusion potential. Now I will explain how this occurs with a thought experiment.

Assume that we have two solutions with different concentrations: high concentration (left) and low concentration (right) (see Figure 2.1). At the boundary between them, the concentration varies like a step function:

$$c\left(x, t=0\right) = \begin{cases} c_{high} \text{ for } x \leq 0. \\ c_{low} \text{ for } x > 0. \end{cases} \tag{2.14}$$

Each solution contains the same number of cations (positive ions C^+, red dots) and anions (negative ions A^-, blue dots). Both solutions are electroneutral, and the net charge in each solution is zero at t = 0 (upper box in Figure 2.1).

Both ion species will diffuse from the high concentrated solution to the low concentrated solution (from left to right in Figure 2.1). Assuming that the ions have different diffusion coefficients, $D_{A-} > D_{C+}$, the flux of A^- will be larger than the flux of C^+.

Shortly after the ions start to diffuse, there has been a net transport of charge (2 blue dots and 1 red dot has moved across the boundary, as seen in the middle box of Figure 2.1). Therefore, a small electric potential

occurs at the boundary, which will counteract further net transport of charge (lower box of Figure 2.1). The potential affects positive and negative ions in opposite ways. The fast anion ions will slow down, while the cation ions will accelerate, such that the ions move at the same speed (lower box in Figure 2.1). Now there is no net movement of charge over the boundary, and the arisen potential is the diffusion potential.
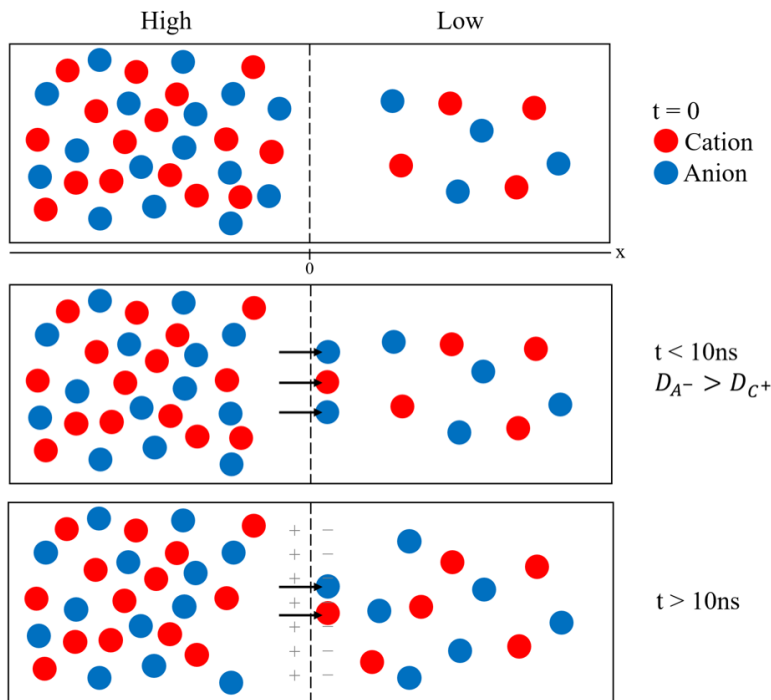
Figure 2.1: Illustration: Thought experiment of how diffusion potentials can occur. Two solutions with high and low concentrations of a cation (red) and an anion (blue) (upper box). The anion has a larger diffusion coefficient and diffuses faster than the cation (net movement of charge, middle box). This creates a potential that is slowing the anion down while speeding up the cation. Now the two ions diffuse at the same speed (lower box).

The time-scale for the potential to appear is within 10 nanoseconds [5]. Concentration changes occur on a much slower time scale (seconds). After the diffusion potential is established, it will change on the same time scale as the concentrations. During the first 10 ns, there is a net transport of charge and a small deviation from electroneutrality. This deviation remains and is the reason for the arisen diffusion potential. The net transport is so small that it does not affect the concentrations significantly. The diffusion potential reaches a quasi-stationary state, where the diffusion current and

the field current balance each other, $\boldsymbol{I}_{\text{diff}} = -\boldsymbol{I}_{\text{field}}$. That is, no net current over the boundary and thereby no accumulation of charge.

The PNP framework models the entire system, including the first 10 ns during the built-up of the potential. On the other hand, the KNP framework neglects the first 10 ns entirely and finds the potential at the quasi-stationary state directly. The system is assumed to be at this quasi stationary state and the diffusion potential can then be found by Equation 2.13. When calculating the diffusion potential, I will use the assumptions made under the KNP formalism.

A last note on the thought experiment and Figure 2.1: If the anion and the cation had equal diffusion coefficients, there would not be any net transport of charge, no occurring potential, and no deviation from electroneutrality. The ions would then diffuse with the same speed until they leveled out the concentration differences.

2.2.2 Calculating the diffusion potential

There are many ways to approximate and calculate the diffusion potential. Two know equations are the Goldman equation and the Henderson equation. In neuroscience, these are mostly used to calculate the potential over neuronal membranes. Then the potential is estimated between two points: the inside and the outside of the membrane.

The neuronal membrane is a lipid bilayer that is impermeable to ions. However, proteins in the membrane make passageways for ions, called ion channels. Ion channels allow certain ions to move across the membrane, and they contribute to the membrane's selective permeability [2]. The membrane separates ion species between the inside (intracellular) and outside (extracellular) of the cells. The most important ion species in the brain are potassium (K^+), sodium (Na^+), chlorine (Cl^-), and calcium (Ca^{2+}). Additionally, there are also ion species such as magnesium (Mg^{2+}) and hydrogen carbonate (HCO_3^-). Table 2.1 show typical values for baseline concentrations of these ion species in the intracellular and the extracellular space. The different ion distribution of the inside and outside leads to a potential across the cell membrane.

When the potential across the membrane is assumed constant it can be determined by the Goldman equation (also called the Golman-Hodgkin-Katz voltage equation) [7]. The potential difference E_m over the neuronal mem-

Table 2.1: Ionic concentrations inside and outside of a mammalian neuron. Values are taken from Somjen (Table 2-1) [6] with ionic concentrations in the central nervous system neurons (intracellular) and in the cerebrospinal fluid (extracellular). These concentration may vary according to different brain regions and species.

Ion	Intracellular [mM]	Extracellular [mM]
K^+	125	2.9
Na^+	10	147
Cl^-	6.6	119
Ca^{2+}	0.00006	1.0
Mg^{2+}	0.5	0.7
HCO_3^-	18	23.3

brane is given by:

$$E_m = \frac{RT}{F} \ln \left(\frac{\sum_{i+} P_i[c_{i+}]_{in} + \sum_{i-} P_i[c_{i-}]_{out}}{\sum_{i+} P_i[c_{i+}]_{out} + \sum_{i-} P_i[c_{i-}]_{in}} \right), \qquad (2.15)$$

where P_i is the membrane permeability of ion species i. Note that the negative ions are inverted relative to the positive ions in the fraction. The Goldman equation can be derived from the Nernst-Planck equation (Equation 2.4), and the diffusion coefficient D is replaced by the permeability P_i (diffusion coefficient of the membrane). With three ions, K^+, Na^+, and Cl^- the Goldman equation becomes

$$E_m = \frac{RT}{F} \ln \left(\frac{P_K[K^+]_{in} + P_{Na}[Na^+]_{in} + P_{Cl}[Cl^-]_{out}}{P_K[K^+]_{out} + P_{Na}[Na^+]_{out} P_{Cl}[Cl^-]_{in}} \right), \qquad (2.16)$$

where P_K, P_{Na}, and P_{Cl} is the membrane permeability to K^+, Na^+, and Cl^-. F is Faraday's constant (96485.3 C/mol), R is the gas constant (8.314 J/mol K) and T is the absolute temperature in units of Kelvin. It is sufficient to use relative permeability for the ions since the permeabilities occur in both numerator and denominator [7]. The relative permeabilities $P_K : P_{Na} : P_{Cl}$ is 1:0.03:0.1 respectively in the squid giant axon [7]. Using the concentrations of K^+, Na^+, and Cl^- from Table 2.1 and a temperature of 37 ^{o}C $\approx$ 310 K, the calculated membrane potential becomes -76 mV. A negative membrane potential tell us that the inside of the neuron is slightly more negative than the outside. When a neuron is in a resting state the potential across the membrane is called the resting membrane potential.

Each ion species has its own reversal potential over the cell membrane because of the concentration gradients. The reversal potential E_k for an ion species k can be calculated with the Nernst equation. The Nernst equation is a special case of the Goldman equation, where the permeability is zero for every ion species except one, and is given as

$$E_k = \frac{RT}{z_k F} \ln \frac{c_{out}}{c_{in}}, \qquad (2.17)$$

where c_{out} is the concentration on the outside and c_{in} is the concentration on the inside of the cell. z_k is the valence of the ion (for K^+ it is +1 and for Cl^-, it is -1). The Nernst equation is an solution of the Nernst-Planck equation when $\boldsymbol{I}_{\text{diff}} = -\boldsymbol{I}_{\text{field}}$ for ion current through an ion channel only permeable to a single ion species k.

Using the Nernst equation (Equation 2.17) with values for K^+ concentrations from Table 2.1 and a temperature of 310 K, the calculated reversal potential of K^+ is -0.1 V or -100 mV. For Na^+, Cl^-, Ca^{2+}, Mg^{2+} and HCO_3^- the reversal potentials are 72 mV, -77 mV, 130 mV, 4 mV, and -7 mV respectively for the concentration values in Table 2.1.

The diffusion potential can also be referred to as a liquid junction potential since the potential is most prominent at the junction or the boundary [8, 9]. Liquid junction potentials can be estimated by the Henderson equation [8, 9]. Strutwolf et al. [8] gives the Henderson equation as

$$\phi_j = \frac{RT}{F} \left(\frac{\sum_i u_i \frac{|z_i|}{z_i} (c_{i,2} - c_{i,1})}{\sum_i u_i |z_i| (c_{i,2} - c_{i,1})} \right) \ln \left(\frac{\sum_i u_i |z_i| c_{i,1}}{\sum_i u_i |z_i| c_{i,2}} \right), \qquad (2.18)$$

where u_i is the mobility of ion species i, z_i is the valence of ion species i, and $c_{i,1}$ and $c_{i,2}$ is the concentration of ion species i in compartment 1 and 2. R is the gas constant, T is the absolute temperature and F is Faraday's constant. The Henderson equation can be derived from the Nernst-Planck equation [8]. The derivation assumes a linear concentration profile within the diffusion layer and it includes the electroneutrality criterion [8].

Perram and Stiles [9] states that the Henderson equation is more promising for calculating potentials over sufficiently thick membranes. When the membrane thickness becomes thinner (nanometers), it is better to use the Goldman equation for calculating potentials [9].

2.3 Extracellular ion concentrations

During neuroscience experiments, the focus is mainly on what happens to the neurons. Therefore, it is often only a few ion concentrations that are measured. The ion species measured are often the ones with the most impact on neuronal activity, such as calcium (Ca^{2+}) or potassium (K^+).

Dramatic ion concentration changes in ECS can occur 'in real life' in somewhat extreme cases, for example, during epilepsy and spreading depression. These can cause rather severe concentration changes. Other 'real life' ECS concentration changes can probably also appear in less extreme cases, for example, during sleep waves and probably to some degree during normal wakeful brain activity.

Concentration changes in ECS can also be evoked artificially by experimental stimuli to selected regions. Ionic concentration changes in ECS can therefore be measured during numerous different situations and conditions.

In this project, I want to find data on extracellular ion concentrations so I can estimate a diffusion potential and calculate PSDs. However, recorded extracellular ion concentrations for more than one ion species are not the easiest to find. This calls for assumptions for concentration changes of unmeasured ion species.

2.3.1 Assumptions on concentrations for unmeasured ion species

Videm [10] proposed five different initial concentration scenarios including three ion species: K^+, Na^+ and Cl^-. Table 2.2 show these five scenarios. For each scenario (except scenario 5), only one ion species is required to calculate the others two. The scenarios are, therefore, very applicable with ECS concentration data.

Scenario 1 states that the change in K^+ is balanced by Na^+. This means that an increase in K^+ leads to an equally large decrease in Na^+. The Cl^- concentration change is zero. In scenario 2, the K^+ increase is equally distributed between Na^+ and Cl^-. Scenario 3 assumes that the change in K^+ is balanced by Cl^- and that the change in Na^+ is zero. In the case of spreading depression, Videm proposed and used scenario 4 [10]. In scenario 4, the change in Na^+ is double the change in K^+ (opposite of each other), and Cl^- is equal to the change in K^+. The fifth scenario is proposed when two ion

Table 2.2: Five scenarios for initial ionic concentrations proposed by Videm [10].

Scenario nr.	Assumption
1	$\Delta[\text{K}^+]^0 = -\Delta[\text{Na}^+]^0 \quad \wedge \quad \Delta[\text{Cl}^-]^0 = 0$
2	$\Delta[\text{K}^+]^0 = -\frac{1}{2}\Delta[\text{Na}^+]^0 + \frac{1}{2}\Delta[\text{Cl}^-]^0$
3	$\Delta[\text{K}^+]^0 = \Delta[\text{Cl}^-]^0 \quad \wedge \quad \Delta[\text{Na}^+]^0 = 0$
4	$2\Delta[\text{K}^+]^0 = -\Delta[\text{Na}^+]^0 \quad \wedge \quad \Delta[\text{K}^+]^0 = -\Delta[\text{Cl}^-]^0$
5	$\Delta[\text{K}^+]^0 + \Delta[\text{Na}^+]^0 = \Delta[\text{Cl}^-]^0$

species are known, and the third ion species is calculated so the electroneutrality criterion is fulfilled.

Videm compared all five scenarios against a simulation of the ideal case by Halnes et al. [1] where all ion concentrations were known. This comparison showed that scenario 5 was closest to the simulation, while scenario 1 was the second-best [10].

Dietzel et al. [11] recorded extracellular concentrations of Na^+, Cl^-, Ca^{2+} and K^+. They managed to measure two ion concentrations simultaneously during experiments: Na^+ and K^+, Na^+ and Ca^{2+}, and Na^+ and Cl^-. The focus of Dietzel et al. [11] was on the dynamics of the ion concentrations. During a stimulus induced activity they found a 1:1 Na^+/K^+ exchange, after correction for Ca^{2+} measurement-interfering [11]. They also found that changes in Cl^- was slow. Dietzel et al. [11] described the conservation of electroneutrality in the extracellular space by

$$[\text{Cl}^-]_e = [\text{K}^+]_e + [\text{Na}^+]_e.$$

Here they assumed that the positive charges remaining in the extracellular space ($[\text{Ca}^{2+}]_e$ and $[\text{Mg}^{2+}]_e$) balances out the remaining negative charge ($[\text{HCO}_3^-]_e$).

Spreading depression and ECS concentration change

Spreading depression (SD) is a transient event often described as a wave of depolarization that can last for minutes [3, 12, 13]. During SD, the activity

in the affected region is suppressed, and there seems to be a prolonged depolarization of the neuronal membranes [12]. In the ECS it can occur a large negative potential shift [12, 13, 14] ranging from 10 mV to 40 mV [13]. SD can occur spontaneously or be evoked by strong stimulation [12, 14].

During spreading depression, there is an accumulation of extracellular K^+ to very high levels [15]. Observations show an initial rise of K^+ concentration to about 10-12 mM preceding concentration decreases in Na^+, Cl^- and Ca^{2+} in the extracellular space [12, 14, 15]. Ayata and Lauritzen [12] emphasized the variability of this K^+ threshold for different brain regions and species.

Sykova and Nicholson [3] observed an increase in tortuosity, λ_n, from $\sim$1.6 to 1.95-2.07 and a decrease in volume fraction, α, from $\sim$0.20 to 0.05-0.09 during spreading depression. Ayata and Lauritzen [12] reports a shrinkage of the extracellular space by more than 50 %.

The accumulation of K^+ occurs because clearing mechanisms in the extracellular space become overloaded [12]. With extensive K^+ efflux the extracellular concentration can reach levels of $\sim$30-50 mM, which is high above the baseline value of $\sim$3 mM [12]. In response, extracellular concentration of Na^+ and Cl^- decrease to $\sim$60 mM and $\sim$75 mM respectively [15]. This decrease is relatively not as dramatic as the increase of K^+ because of their respective baseline concentrations. The huge rise in K^+ is important for the spreading of the depolarizing wave. This is because the K^+ concentration is large enough to depolarize neighboring cells [12].

Kraig and Nicholson [14] discovered an equality in the concentration changes of Na^+ and Cl^- during experiments of spreading depression: Na^+ and Cl^- seemed to decrease with similar amount. If only K^+ and Cl^- were measured, the change in Na^+ can be calculated from Cl^- change as

$$[Na^+] = [Na^+]_{\text{base}} - \Delta[Cl^-], \quad (\Delta[Na^+] = \Delta[Cl^-]). \qquad (2.19)$$

To fulfill the electroneutrality requirement, they introduced an anion deficit A^- which is calculated from the concentrations of K^+, Na^+ and Cl^-:

$$\Delta[A^-] = \Delta[K^+] + \Delta[Na^+] - \Delta[Cl^-]. \qquad (2.20)$$

Figure 2.2 shows the temporal concentration changes of K^+, Na^+, Cl^-, and A^- during spreading depression. The anion deficit A^- reflects the changes in K^+ since the changes in Na^+ and Cl^- are equal. From Figure 2.2 we also see that Cl^- and Na^+ change with $\sim$100 mM while K^+ and A^- changed with
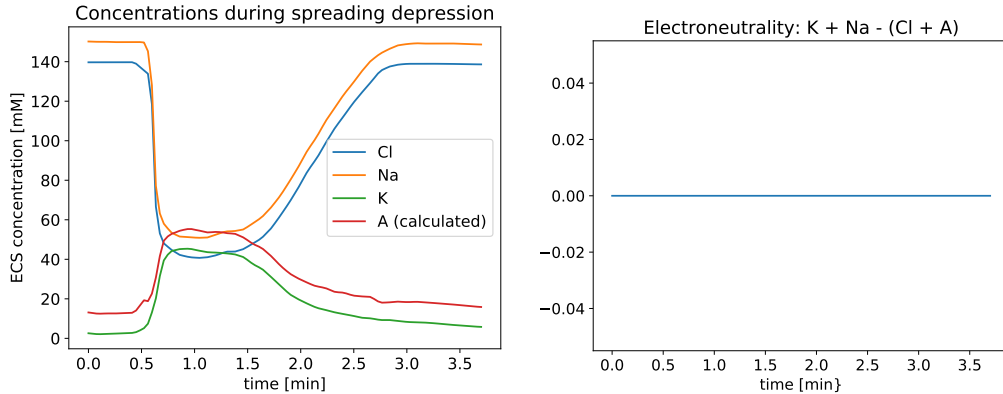
Figure 2.2: ECS concentration changes during spreading depression. Left: ion concentration changes over time. Na^+ is calculated from Cl^- and A^- is included to maintain electroneutrality. Data is taken from Kraig and Nicholson (Fig. 8) [14]. Right: Checking the electroneutrality criterion.

about 40 mM. Scenario 4 from Videm [10], where Na^+ change is assumed to be two times the K^+ change, is somewhat supported by this.

2.3.2 Assumptions on decay times for ion concentrations in ECS

The diffusion potential is an instant function of the concentration gradients. The potential will therefore change when the gradients change. Videm [10] estimated the diffusion potential from the change of concentration gradients due to diffusion. The concentration gradients can also change because of various uptake mechanisms in neurons and glial cells.

The time course of K^+ concentration decay in the ECS may tell something about how fast the diffusion potential changes. Cordingley and Somjen [16] studied half-decay times of extracellular K^+ in the cortex and spinal cord of cats. They found out that the half-decay time calculated for diffusion was more than a hundred times longer than half-decay times observed for K^+ transients in ECS [16]. Such may indicate that other uptake mechanisms contribute the most to the K^+ decay in ECS and that the K^+ decay not only can result from a diffusion process.

Cordingley and Somjen [16] also investigated if the depth of recording affected the half-decay times of K^+. The result was similar half-decay times in all depths, but in the center, where the K^+ concentration was highest, the half-decay time was slightly shorter [16].

16

2.4   Local Field Potentials

Potentials in the extracellular space are affected by the activity of surrounding neurons. ECS potentials are measured relative to a reference point by small electrodes inserted in the brain [17]. The extracellular potential is often divided into a high-frequency part and a low-frequency part.

Neuronal action potentials are fast-changing signals, and information about them is visible in the high-frequency part (>300Hz) [18]. This part of the extracellular potential is called the Multi-Unit Activity (MUA), and it contains firing information from the surrounding neurons. Local field potential (LFP), on the other hand, is the low-frequency part of the ECS potential. LFP contains frequencies below ∼250 Hz and reflects current flow associated with synaptic activity [18].

Comparing different LFP measurements is difficult since they often appear to be similar. It is hard to discover underlying patterns in the measurements. Therefore, it can be easier to compare the dominant frequency components of the LFPs. One way of doing so is to calculate and compare the power spectrum densities of the LFPs.

2.5   Power spectrum density

The power spectrum density (PSD) is often used in signal analysis. The goal of using PSD is to make time-varying signals more comparable by looking at which frequencies that dominates the signals. The PSD of a signal represents the signal's frequency components.

The first step in obtaining the PSD is to calculate the Fourier transform, $\mathcal{F}(f)$, which is defined as

$$\mathcal{F}(f) = \int_{-\infty}^{\infty} v(t) e^{-i2\pi f t} dt, \tag{2.21}$$

where $v(t)$ is the time-dependent signal we want to transform. As seen from the equation, the Fourier transform is frequency-dependent, and the original signal $v(t)$ is transformed from the time domain to the frequency domain. $\mathcal{F}(f)$ can be said to be the frequency spectrum of the signal $v(t)$ [19].

An assumption of the Fourier transform is that $v(t)$ is an continuous function [19]. To extend the Fourier transform, to cases where $v(t)$ is given as values at finitely many points, one can apply the Discrete Fourier Transform

(DFT). To make the number of computations manageable for large data sets, the DFT can be computed by a method called the Fast Fourier transform (FFT) [19].

The values returned by the FFT is on complex form, they have both a real and an imaginary part [20]. The next step is therefore to find the magnitude (the absolute value) of the FFT to be able to do further analysis (in complex analysis also known as $(z^*z)^{1/2}$ where z is a complex number and z^* is the complex conjugate of z). After finding the magnitude of the FFT, we must normalize it by dividing it by its own length N (which in certain cases is equal to the sampling frequency f_s).

The sampling frequency (also called sampling rate) is the number of samples obtained per unit of time. For example, a sampling frequency of 1250 Hz means that it is sampled 1250 samples per second.

From the FFT we get a two-sided spectrum containing both positive and negative frequencies [20]. Normally we only look at the positive frequencies, because the spectrum of a real-world signal is symmetric around 0 Hz (often called DC). To do so we discard the negative frequencies, which are the second half of the two-sided spectrum. To obtain the total energy in the spectrum, we must multiply all points in the positive frequencies, except 0 Hz (DC), by two [20]. The resulting spectrum is called a single-sided spectrum and has the frequency range of $[0, f_s(0.5 - 1/N)]$ (f_s is the sampling frequency and N is the number of points returned by FFT/number of points in the original signal) [20].

If we stop here, we have calculated the amplitude spectrum:

$$\text{Amplitude spectrum} = 2\frac{|\mathcal{F}(f)|}{N} \quad , \quad f \in (0, f_s(0.5 - 1/N)] \qquad (2.22)$$

Note that at 0 Hz (DC) the amplitude spectrum is calculated by dropping the 2 in the above equation: $\frac{|\mathcal{F}(f)|}{f_s}, f = 0$ Hz.

To calculate the power spectrum (PS), the only difference is that we must square the normalized magnitude of the FFT. The equation for power spectrum (PS) is

$$\text{PS} = 2\left(\frac{|\mathcal{F}(f)|}{N}\right)^2 \quad , \quad f \in (0, f_s(0.5 - 1/N)]. \qquad (2.23)$$

Here $\mathcal{F}(f)$ is the Fast Fourier transform and f_s is the sampling frequency. As

with the amplitude spectrum, the PS at $f = 0$ Hz is calculated by removing 2 from the formula.

Here comes a quick refresh of the steps to calculate the power spectrum (PS): find the absolute value/the magnitude of the FFT, normalize it by dividing on its length, square it and multiply by two. Then, discard the second half of the frequencies [20], which is specified by the frequency range.

The power spectrum density (PSD) is now easily calculated by dividing PS by the frequency bin $df = f_s/N = 1/(N \cdot dt)$:

$$\text{PSD} = \frac{PS}{df} = \frac{PS \cdot N}{f_s} = \frac{2N}{f_s}\left(\frac{|\mathcal{F}(f)|}{N}\right)^2 \quad , \quad f \in (0, f_s(0.5 - 1/N)]. \quad (2.24)$$

If the original signal is in volt (V) the unit of the amplitude spectrum is volt. The units of PS become V^2 and the unis of PSD become V^2/Hz. (The formulas in this section are found by combining information from a tutorial [20] and a forum[1].)

2.5.1 Simple PSD example

To illustrate the power spectrum density, I calculated it for a superposition of four sine waves. The superposition is composed of four sine waves with different frequencies and amplitudes:

$$v(t) = sin(1 \cdot 2\pi t) + 0.5sin(5 \cdot 2\pi t) + 0.1sin(10 \cdot 2\pi t) + 0.2sin(30 \cdot 2\pi t)$$

The four sine waves are shown individually in the upper left of Figure 2.3. Here they have the same amplitude but different frequencies: 1, 5, 10, and 30 (from top to bottom). The superposition $v(t)$ of the sine waves are shown in the upper right of Figure 2.3, and the amplitudes for each sine wave are 1, 0.5, 0.1, and 0.2 respectively.

The amplitude spectrum and power spectrum density are shown in the lower panel of Figure 2.3. The amplitude spectrum (lower left of Figure 2.3) shows the amplitude for each frequency component, and the peak values correspond with the amplitudes in the superposition. The power spectrum density (lower right of Figure 2.3) has peak values at the same frequencies, but the power amplitudes are smaller than in the amplitude spectrum. The

---

[1]The forum is avaiable at: https://stackoverflow.com/questions/22338415/scipy-periodogram-terminology-confusion (Accessed: 21 April 2021)

peak value of the power amplitude can be found with the following equation:

$$\text{Power Amplitude} = \left(\frac{A}{\sqrt{2}}\right)^2 = \frac{A^2}{2},$$

where A is the amplitude of a sine wave in the superposition. For the amplitudes 1, 0.5, 0.1 and 0.2 the power amplitude become 0.5, 0.125, 0.005 and 0.02 respectively. This can be seen in the lower right panel of Figure 2.3.
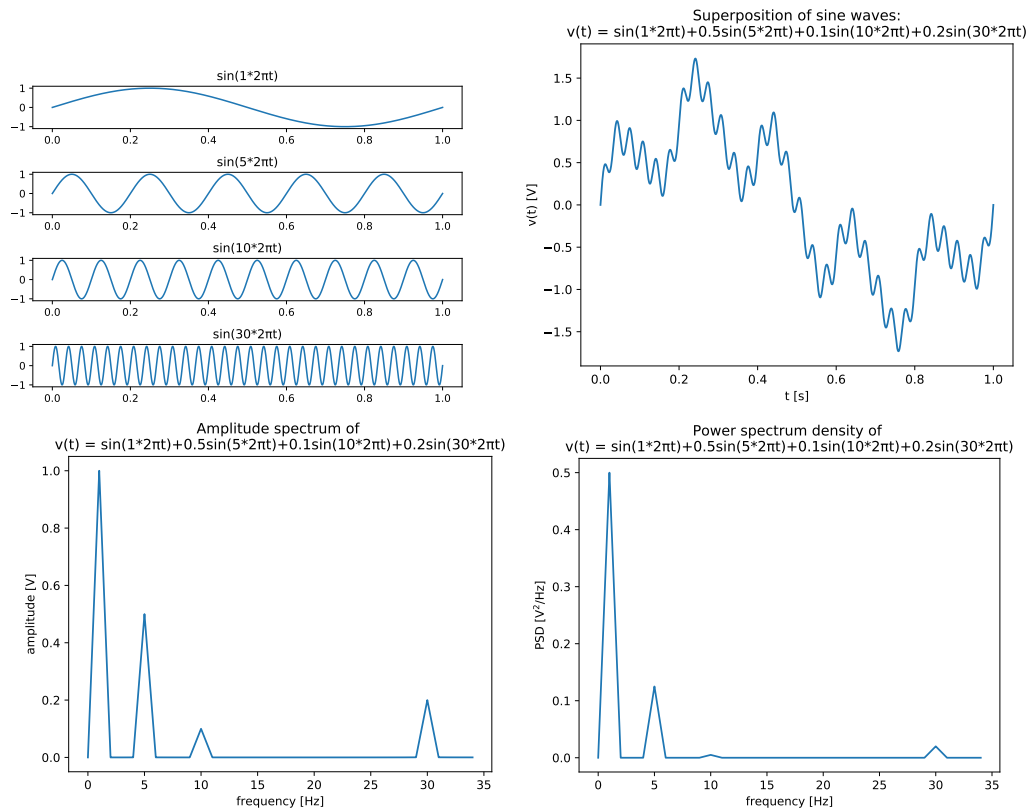

Figure 2.3: Upper left: Four sine waves with different frequencies: 1, 5, 10 and 30. Upper right: The superposition of the four sine waves with different amplitudes: 1, 0.5, 0.1 and 0.2. Lower left: The amplitude spectrum of the superposition, with peaks at the four frequencies. Lower right: The power spectrum density of the superposition, with peaks at the four frequencies and power amplitudes of 0.5, 0.125, 0.005 and 0.02. The units of the superposition and the amplitude spectrum is volt, while the PSD has units V^2/Hz.

The PSD of the signal shows how the peaks in the PSD appear at the four frequencies in the superposition. We can also see that the largest power is at the frequency component with the largest amplitude.

2.5.2 PSDs in previously published articles

In previously published articles, the LFP measurements are often presented as power spectrum densities. The units of the PSDs are in many articles unclear. The PSDs are often shown with arbitrary units or units entirely omitted. Therefore, it is difficult to say something about the magnitude of the original LFP signal. In addition, comparing two PSDs with arbitrary or different units is inadequate.

Luckily there exist data sharing tools such as the Collaborative Research in Computational Neuroscience (CRCNS)[2]. CRCNS is a site for data sharing across the world in the field of neuroscience. This site gives researchers and experimentalists the ability to share their data. Non-experimentalists can also get a hold of data sets without executing the experiments themselves. The only requirement for downloading data sets is to have a CRCNS-account. CRCNS contains numerous data set from many brain regions, to mention some of them: visual cortex, auditory cortex, prefrontal cortex, motor cortex, somatosensory cortex, hippocampus, thalamus, basal forebrain, and cerebellum.

In this project, I have used the CRCNS data sharing site to download LFP recordings, and then calculated PSDs directly from those.

---

[2]Available at: `https://crcns.org/` (Accessed: 27 April 2021)

Chapter 3

Methods

In this project, I investigated diffusion potentials' undetermined impact on local field potentials (LFPs). My approach to the project is illustrated in Figure 3.1.
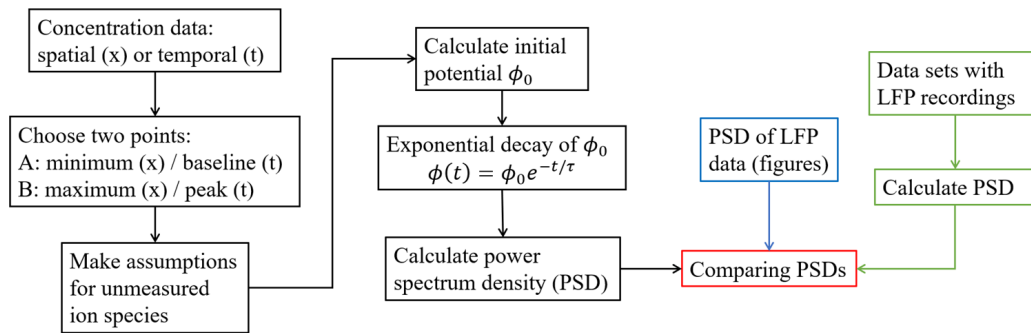

Figure 3.1: Project approach.

For concentration data: I collected data from published articles and selected two concentration points, A and B, for further use (Section 3.1 and 3.2). Based on certain assumptions, I calculated concentrations for unmeasured ion species I wanted to include (Section 3.3). I estimated the diffusion potential ϕ_0 and its exponential decay (with τ from temporal concentration data) (Section 3.4 and 3.5). Finally, I calculated the power spectrum densities (PSDs) of the potentials (Section 3.6). (black boxes in Figure 3.1).

For LFP data: I collected LFP data presented as PSDs in figures from published articles (blue box in Figure 3.1). In addition, I found LFP recordings from data sets and calculated PSDs directly from those (green boxes in Figure 3.1, Section 3.7).

The comparison of the PSDs are presented in Chapter 4 (red box in Figure 3.1). The method chapter is structured as indicated in Figure 3.1.

3.1 Concentration data

Ion concentration data in ECS can be presented as spatial or temporal data. In spatial data, the ion concentrations are measured in different depths at one point in time, for example, in the different layers of the cortex. For temporal data, the ion concentrations are measured at a fixed point over time, often before, during, and after a given stimulus. I found temporal data to be the most common representation of ion concentrations in the ECS in articles.

I found and divided concentration data into two categories: "normal" (non-pathological) and "pathological" (spreading depression and seizures). For most of the concentration data, I zoomed in and read the figures by visual inspection. To read some of the more detailed figures, which I wanted to reconstruct, I used a web-based tool called WebPlotDigitizer[1] to extract the data points. Here I uploaded the figure as an image and defined and calibrated the axis. I created data sets by marking the data points in the figure and downloaded the data sets as csv-files.

Figure 3.2 show K^+ concentration data (both spatial and temporal) during repetitive stimulation (left) and during spreading depression (right).
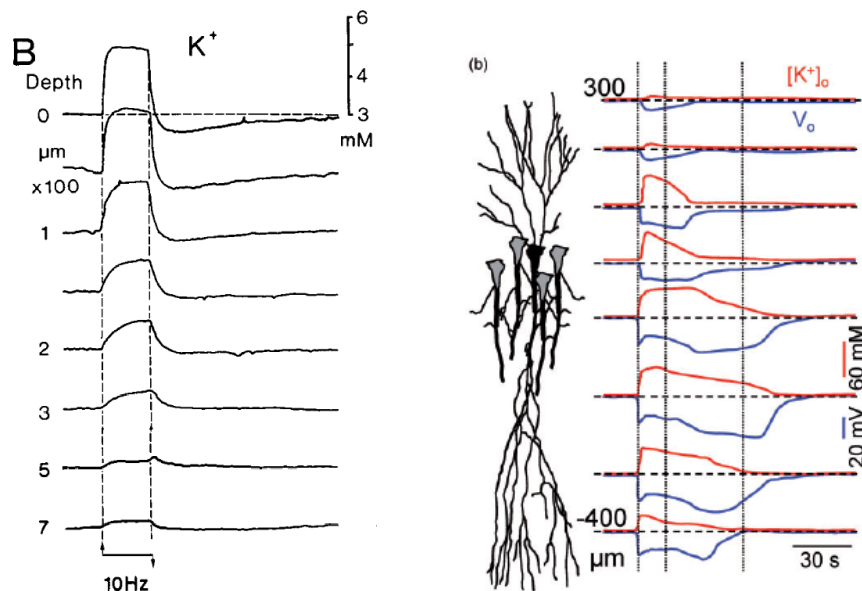

Figure 3.2: Spatial and temporal K^+ concentration data in the ECS. Left: during repetitive stimulation, taken from Nicholson et al. (Fig.2B) [21]. Right: during spreading depression (red lines), taken from Herreras and Makarova (Fig.1b) [13].

---

[1]WebPlotDigitizer: `https://apps.automeris.io/wpd/` (Accessed: 28 April 2021)

3.2   Choosing two points: A and B

The main simplification of this project is that I chose to work with only two points, A and B, from the concentration data. Point A stand for the baseline concentration, c_{base}, or the minimum concentration difference from baseline, Δc_{min}. I chose to look only at the extreme cases, such that Point B denotes the maximum concentration difference from baseline, Δc_{max}.

For spatial data, I chose point A as the minimum difference from baseline and point B as the maximum difference from baseline (see left panel of Figure 3.3). For the previous Figure 3.2 (left panel) point A would be at 700 μm depth and point B at depth 0. For the right panel of Figure 3.2 I would choose point A at 300 μm depth and point B as the fifth depth-line from the top.
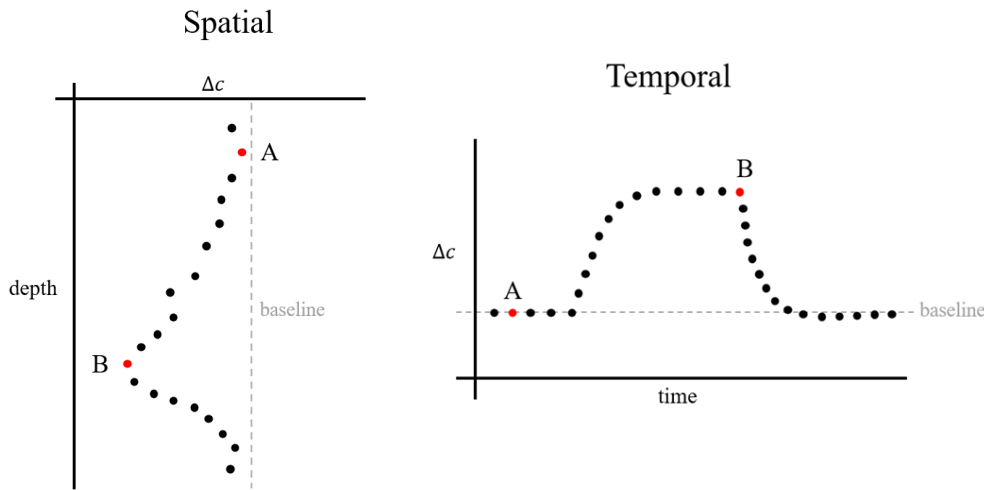
Figure 3.3: The figure show how I chose point A and B for spatial (left) and temporal (right) data.

For temporal data, I chose point A as the baseline concentration (the 'before' concentration) and point B as the peak concentration (see right panel of Figure 3.3). I assumed that these two points exist simultaneously and spatially separated in the ECS. The previous Figure 3.2 have temporal concentration data for each depth line, and I would choose points A and B as shown by the right panel of Figure 3.3.

3.3 Determining concentrations for unmeasured ion species

In articles, a large amount of concentration data often only include one ion species, sometimes two ion species. For my calculations, I chose to include the ion species K^+, Na^+, and Cl^-. Using these three ions, I based the concentration change of two of them on only one ion species. For "normal" concentration data I used scenario 1 from Videm[10] (presented in Section 2.3.1):

$$\Delta[K^+]^0 = -\Delta[Na^+]^0 \quad \wedge \quad \Delta[Cl^-]^0 = 0, \tag{3.1}$$

where change in K^+ concentration is balanced out by Na^+ and Cl^- concentration change is assumed to be zero. For "pathological" concentration data, I used scenario 4 from Videm [10] (presented in Section 2.3.1):

$$2\Delta[K^+]^0 = -\Delta[Na^+]^0 \quad \wedge \quad \Delta[K^+]^0 = -\Delta[Cl^-]^0, \tag{3.2}$$

where change in concentration of Cl^- is equally large as K^+ and change in Na^+ is double but opposite of the change in K^+.

Regarding baseline ionic concentrations in ECS, I used the baseline values specified with the concentration data. For the cases where I found no specified baseline concentration, I assumed and used the baseline concentration showed in Table 3.1 (K^+ and Na^+ is taken from Table 2.1 on page 11 [6]).

Table 3.1: Baseline concentration values for ion species in ECS used in calculations. Cl^-_{base} is calculated from $K^+_{base} + Na^+_{base}$ to maintain the electroneutrality criterion.

Ion	ECS baseline
K^+_{base}	3 mM
Na^+_{base}	147 mM
Cl^-_{base}	150 mM

3.4 Calculating the diffusion potential

I calculated the diffusion potentials in three alternative ways, based on (1) the Goldman equation, (2) the Henderson equation, and (3) an approximated

equation for $\Delta\Phi$ using the conductivity σ. In this section, I present the equations, and a comparison of their predictions is presented in Chapter 4.

3.4.1 The Goldman equation

To use the Goldman equation for estimating the diffusion potential, I replaced the permeability parameter with the diffusion coefficient. I assumed that the membrane permeability of an ion species is the ion's diffusion coefficient through the membrane. The Goldman equation used to calculate the diffusion potential in the ECS is:

$$\Phi_G = \frac{RT}{F} \ln\left(\frac{\sum_{i+} D_{i+}^* [c_{i+}]_A + \sum_{i-} D_{i-}^* [c_{i-}]_B}{\sum_{i+} D_{i+}^* [c_{i+}]_B + \sum_{i-} D_{i-}^* [c_{i-}]_A}\right), \tag{3.3}$$

where D_i^* is the diffusion coefficient for ion species i in ECS. $[c_i]_A$ and $[c_i]_B$ are the extracellular concentration of ion species i in point A and point B. I termed the diffusion potential calculated with the Goldman equation as Φ_G.

3.4.2 The Henderson equation

To use the Henderson equation for estimating the diffusion potential, I replaced the mobility parameter with the diffusion coefficient. According to the Einstein Relation ($\mu = D_i z_i F / RT$), the relative difference between the mobilities is equivalent to the relative difference between diffusion coefficients for the same ion species. Therefore, I substituted the diffusion coefficient into the Henderson equation as follows:

$$\Phi_H = \frac{RT}{F} \left(\frac{\sum_i D_i^* \frac{|z_i|}{z_i} (c_{i,B} - c_{i,A})}{\sum_i D_i^* |z_i| (c_{i,B} - c_{i,A})}\right) \ln\left(\frac{\sum_i D_i^* |z_i| c_{i,A}}{\sum_i D_i^* |z_i| c_{i,B}}\right), \tag{3.4}$$

where D_i^* is the diffusion coefficient of ion species i in ECS. $c_{i,A}$ and $c_{i,B}$ are the concentration of ion species i in point A and B. I termed the diffusion potential calculated with the Henderson equation as Φ_H.

Table 3.2 shows mobility values (estimated by Strutwolf et al. [8]) and diffusion coefficients to K^+ and Na^+. I checked the ratios between the mobilities and the diffusion coefficients for these ion species. The diffusion coefficients ratio, D_{Na}/D_K, is 0.67857, and the mobilities ratio, μ_{Na}/μ_K, is 0.68101. The

ratios are close to each other. The small difference is most likely due to some variation in the decimals of the constants.

Table 3.2: The diffusion coefficient of Na$^+$ and K$^+$ [1, 10] and the mobility of the same ions calculated by Strutwolf et al. (in Table 1) [8]. The last row shows the ratio between the diffusion coefficients (D$_{Na}$/D$_K$) and the ratio between the mobilities (μ_{Na}/μ_K).

Ion	Diffusion coefficient, D$_{ion}$	Mobility, μ_{ion}
Na$^+$	1.33×10^{-9} m^2 s^{-1}	4.59×10^{-4} cm^2 s^{-1} V^{-1}
K$^+$	1.96×10^{-9} m^2 s^{-1}	6.74×10^{-4} cm^2 s^{-1} V^{-1}
Na$^+$ / K$^+$	0.67857	0.68101

3.4.3 Approximated equation

I also computed the diffusion potential using a third equation, based on an approximation of the potential gradient $\nabla\Phi$ and the concentration gradient ∇c_k used in Equation 2.13 (see page 8). First, I assumed that the gradients were in only one direction, and then I approximated the derivatives as follows:

$$\nabla\Phi \rightarrow \frac{d\Phi}{dx} \approx \frac{\Delta\Phi}{\Delta x} \approx \frac{\Phi_B - \Phi_A}{\Delta x}, \tag{3.5}$$

$$\nabla c_k \rightarrow \frac{dc_k}{dx} \approx \frac{\Delta c_k}{\Delta x} \approx \frac{c_{k,B} - c_{k,A}}{\Delta x}. \tag{3.6}$$

Next, I substituted these approximations into Equation 2.13 and rearranged the equation to get an expression for $\Delta\Phi$:

$$\Delta\Phi = \frac{F}{\sigma}\sum_k z_k D_k^* \Delta c_k. \tag{3.7}$$

where $\Delta\Phi = \Phi_B - \Phi_A$ and $\Delta c_k = c_{k,B} - c_{k,A}$. The summation is over all ion species k and σ is the conductivity (see Equation 2.10 on page 7).

For my two-point system, I also approximated the conductivity, σ. I used an average conductivity, $\bar{\sigma}$, and replaced the concentration c_k with the average concentration of the two points, $(c_{k,A} + c_{k,B})/2$. The equation for average conductivity became:

$$\bar{\sigma} = \frac{F}{\Psi}\sum_k D_k^* z_k^2 \frac{(c_{k,A} + c_{k,B})}{2}, \tag{3.8}$$

where $c_{k,A}$ and $c_{k,A}$ is the concentration of ion species k in point A and B respectively. The average conductivity approximation is most valid when the conductivities of the two points are similar. I included Equation 3.7 as a two-point version of Videm's [10] numerically solution of the time dependent Nernst-Planck equation (Equation 2.6 on page 6). The reason for this was so I could compare the way one normally discrete and solve differential equations for spatial diffusion systems.

3.5 Exponential decaying potential

The equations in the last section are my options for estimating the initial diffusion potential, Φ_0, directly from concentration data together with assumptions for the unmeasured ion species. To estimate how the diffusion potential change with time, I chose to look at the decay of the potential.

The diffusion potential depends solely on the concentration differences between two points. It does not depend on how the difference occurred or changes over time. The potential is an instant function of the ion concentrations in point A and point B. There is no requirement that a diffusion process must have happened to get a diffusion potential.

I simulated the diffusion potential over time with an exponentially decaying function. I estimated the initial potential, Φ_0, and used a time constant, τ, for its exponential decay, as follows:

$$\Phi(t) = \Phi_0 \cdot e^{-t/\tau}.\tag{3.9}$$

Here $\Phi(t)$ is the time series of the potential during time t. With this exponentially decaying potential, I did not assume that diffusion is the only process contributing to the changing potential. Other things contribute to concentration change in the ECS, such as uptake by neurons and glial cells through ion channels and pumps [2].

From temporal concentration data, I found time constants for the concentration decay back to baseline. I chose to use such time constants for the estimated initial potential to ensure a somewhat realistic potential reduction over time.

For most of the concentration data, I found the time constant by visual inspection of the figures. I used the time scales and concentration scales on the figure and found the point where the concentration had decayed to

$1/e \approx 0.368$ of its peak value. I chose to focus on the decay time constant, but the same could be done for the rise to the peak value. Then one finds the point where the concentration reached $1 - 1/e \approx 0.632$ of the rise to the peak value.

In Figure 3.4 I recreated the temporal K^+ concentration data found in Haj-Yasein et al. [22], during and after synaptic stimulation. The blue dots are the K^+ concentration in ECS and the lines are exponentially decaying functions, $c(t) = c_0 e^{-t/\tau}$, with different time constants τ. The exponentially decaying functions seem to fit the concentration data well in the left panel of Figure 3.4. The concentration decay in the right panel of Figure 3.4 does not fit the exponential functions that well, but it still seems to be an acceptable approximation for the decay. Therefore, I assumed that I could use the time constants found from concentration data to estimate how the diffusion potentials decay with time.
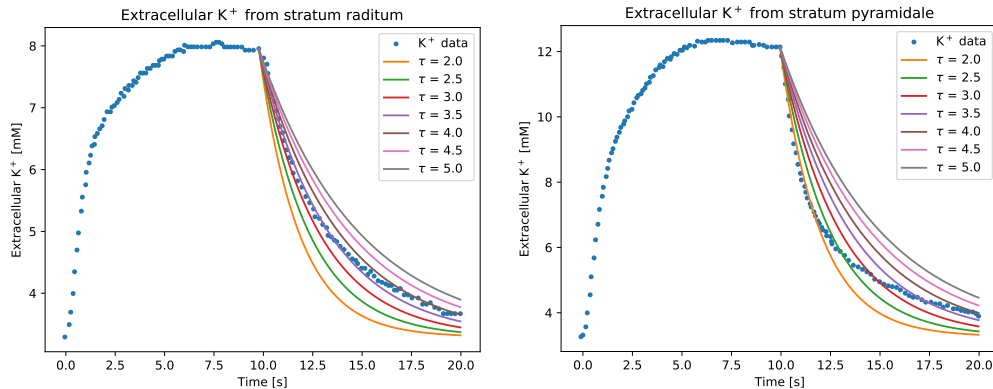

Figure 3.4: Time recordings of K^+ during synaptic stimulation in mouse hippocampus [22]. The blue points are recorded in a wild mouse from Haj-Yasein et al. [22] (Fig.2a (left) and Fig.2b (right)). The lines starting at the point of decaying is exponential curves with different time constants.

3.6 Calculating Power Spectrum Density

For calculating the power spectrum density (PSD) of a time series (here the exponentially decaying diffusion potential), I used the `periodogram`[2] function from SciPy's `signal` package. I inserted the time series and the sampling

---

[2]Link to the documentation: `https://docs.scipy.org/doc/scipy/reference/generated/scipy.signal.periodogram.html` (Accessed: 7 April 2021)

frequency into the `periodogram` function. The `periodogram` returns an array of sample frequencies with the corresponding power spectrum density of the time series. For viewing and comparing PSDs, I plot them on a log-log scale.

Looking into the source code[3] for the `periodogram`, I discovered that the function uses Welch's method[4] when estimating the PSD. This method divides the data into overlapping segments and calculates the PSD individually for each segment [23]. Then, all the segment periodograms are averaged [23], which minimizes edge effects.

The `periodogram` function can calculate both power spectrum (PS) and power spectrum density (PSD). The `scaling` parameter of the function regulates the output. `scaling='spectrum'` computes PS with units V^2, and `scaling='density'` computes the PSD with units V^2/Hz (assuming the units of the time series are volts, V, and that the sampling frequency is in Hz). A forum[5] discussed this scaling parameter, and the default value is `scaling='density'`, which is what I used to calculate PSDs.

3.7   PSD data

Finding power spectrum density data is a bit more challenging than concentration data. Most figures showing PSDs of LFP data have arbitrary units, or they are represented with normalized power. Both cases make it difficult to compare PSDs across articles, and therefore I can not use such figures. I looked for PSDs with the unit V^2/Hz, so I could compare PSD data from figures to the calculated PSDs of the diffusion potentials. As with some of the concentration data, I used the WebPlotDigitizer[6] to extract the PSD data from figures.

I also looked for data sets with LFP recordings from the Collaborative Research in Computational Neuroscience (CRCNS). After some preprocessing of the data in MATLAB, I saved LFP data to files and calculated the

---

[3]Source code available at: `https://github.com/scipy/scipy/blob/v1.6.2/scipy/signal/spectral.py#L158-L288` (Accessed: 8 April 2021)

[4]SciPy's signal.welch function: `https://docs.scipy.org/doc/scipy/reference/generated/scipy.signal.welch.html` (Accessed: 8 April 2021)

[5]The forum is avaiable at: `https://stackoverflow.com/questions/22338415/scipy-periodogram-terminology-confusion` (Accessed: 21 April 2021)

[6]Link to WebPlotDigitizer: `https://apps.automeris.io/wpd/` (Accessed: 28 April 2021)

mean PSD with the `peridogram` function in Python. An overview of the data sets I used is presented in Chapter 4.

In some of the data sets, the LFP recordings were stored in binary files. To read these data files, I used a MATLAB script called `LoadBinary.m`, which I obtained from MATLAB script files belonging to the data set called hc-2 (the data sets and their names are presented in more detail in Section 4.5.2). For LFP data stored in binary files, I needed to convert the data into units of volts[7]. To do so, I used a conversion factor X found by

$$X = \text{VoltageRange} /(\text{nBits} * \text{gain}), \qquad (3.10)$$

where VoltageRange, nBits, and gain are parameters following the data set. nBits depend on the binary file storage (if stored with 16 bits, nBits $= 2^{16}$), and gain is the same as amplification of the signal. I multiplied the data with the conversion factor to get units of volts: Data $*$ X. (If there is an offset in the data set, I subtracted it before multiplying: (Data-Offset) $*$ X)

The data sets from CRCNS have LFP data recorded over multiple channels. I wanted to calculate the mean PSD. Therefore, I computed the PSD for each channel and then found the mean PSD by taking the average over all the PSDs.

3.8 Table of constants

Table 3.3 contain all the constants used in this project.

Table 3.3: List of constants [1, 10].

Symbol	Value	Explanation
D_{Na}	$1.33 \cdot 10^{-9}$ m^2/s	Na$^+$ diffusion coefficient
D_K	$1.96 \cdot 10^{-9}$ m^2/s	K$^+$ diffusion coefficient
D_{Cl}	$2.03 \cdot 10^{-9}$ m^2/s	Cl$^-$ diffusion coefficient
F	96485.333 C/mol	Faraday's constant
R	8.3144598 J/mol K	Gas constant
T	310 K	temperature (considered constant)
λ_n	1.6	tortuosity

---

[7]How to convert to volt is discussed in this forum: `http://crcns.org/forum/using-datasets/708216874` (Accessed: 19 March 2021)

3.9   Code available on GitHub

The Python code used in this project is available on my GitHub repository:
`https://github.com/christinebr/Master-Project-2021`.   The original
data sets of the LFP recordings are not uploaded because of the file sizes.
However, I uploaded files containing the calculated PSD that I used to plot
the figures in Chapter 4.

Chapter 4

Results

4.1 "Normal" concentration data

The concentration data collected are shown in Table 4.1 on page 36. In the table, the concentration data is labeled with the article's first author and the figure I used. For each data set, the concentration data is presented with corresponding decay time constant, and some additional information. I divided the concentration column into three to specify the ion species, the baseline concentration, and the maximum concentration difference, Δc. The baseline concentration is found from the article, otherwise I used the values specified in Table 3.1 (on page 26).

If I managed to find the time constant for the decay back to base concentration, it is in the table. Otherwise, for example, if the concentrations were a depth profile, no time constant is shown. In these cases, I used a time constant of 6 s if not otherwise indicated in the 'Note' column.

Table 4.1: "Normal" concentration data. The table shows where data is taken from, the extracellular concentration of an ion (with baseline and maximum difference Δc), and the corresponding time constant for the ionic concentration decay. Some additional information about the data is provided under the 'Note' column.

Taken from	Concentrations (ion, base, Δc) [mM]	Time constant, τ_{decay} [s]	Note
Dietzel Fig 3 [11]	Na^+, 146, -5.9	-	depth profile
Dietzel Fig 4A [11]	K^+, 3, +6	$\sim 4s$	stimulation of cortical
Dietzel Fig 4B [11]	K^+, 3, +7	$\sim 6s$	surface, adult cats
Hay-Yasein Fig 2a [22]	K^+, 3.25, +4.75	$\sim 3.0s$	recordings from stratum radiatum, mice
Hay-Yasein Fig 2b [22]	K^+, 3.25, +9.25	$\sim 2.5s$	recordings from stratum pyramidale, mice
Cordingley Fig 5 [16] (Gratiy Fig 2B [24])	K^+, 2.6, +1.89	-	depth profile, cortical layers in cat, half-decay time of 0.52s ($\tau \approx 0.75s$)
Sykova Fig 3A [25]	K^+, 3, +6	$\sim 12s$	tetanic stimulation of posterior tibial nerve recorded in spinal cord of cat
Sykova Fig 14A [25]	K^+, 3, +5	$\sim 4s$	cerebellar stimulation at 20 Hz, measured in rat cerebellum
McCreery Fig 2B [26]	K^+, 3, +4	$\sim 25s$	recorded in postcruciate gyros of cat
Halnes2016 [1] (Videm Fig 2.4 [10])	K^+, 3, +5.99	-	depth profile, simulated using 10 pyramidal neurons
Nicholson Fig 3 [21]	K^+, 3, +5	$\sim 20s$	repetitive stimulation, cat cerebellar cortex
Octeau Fig 1G [27]	K^+, 4.5, +0.9	$\sim 6s$	response to light flash, mice
Amzica Fig 3A [28]	K^+, 3.4, +0.6	-	slow oscillation ($\sim 2s$), wave-triggered averages, cerebral cortex of cats
Frölich2008 Fig 1B [29]	K^+, 3, +1.6	-	slow oscillation ($\sim 2s$), suprasylvian gyrus of cat

4.2 Comparing the equations and the scenarios

Here, I present a comparison of the predictions from the three equations discussed in Chapter 3 (see Section 3.4 on page 26) for scenario 1 and scenario 4 (see Section 3.3). I assumed different K^+ concentration differences from baseline (Δc is +2, +4, +6, and +9). I used the scenarios to find Δc for Na^+ and Cl^-. The estimated diffusion potentials are calculated between point A (baseline) and point B (maximum difference Δc). Table 4.2 show the estimated values from the Goldman equation (Equation 3.3), the Henderson equation (Equation 3.4), and the approximated equation (Equation 3.7).

Table 4.2: Calculating the potential with the Goldman equation, the Henderson equation and the approximated equation (with average conductivity, σ). All calculations are based on a K^+ concentration difference from baseline, and the Na^+ and Cl^- concentrations are found from scenario 1 and scenario 4. Concentration values are given in millimolar (mM) and potential values are given in millivolts (mV).

Scenario 1

$\Delta[K^+]$ [mM]	+2	+4	+6	+9
Goldman, Φ_G [mV]	-0.06558200	-0.13100340	-0.19626497	-0.29385936
Henderson, Φ_H [mV]	-0.06558200	-0.13100340	-0.19626497	-0.29385936
Approx, $\Delta\Phi$ [mV]	0.06558197	0.13100314	0.19626409	0.29385640

Scenario 4

$\Delta[K^+]$ [mM]	+2	+4	+6	+9
Goldman, Φ_G [mV]	-0.13936351	-0.28022935	-0.42262393	-0.63914161
Henderson, Φ_H [mV]	-0.13936453	-0.28023761	-0.42265226	-0.63923961
Approx, $\Delta\Phi$ [mV]	-0.28606129	-0.57520233	-0.86747313	-1.31185968

For scenario 1, all the equations gave very similar estimates for the potential. The Goldman equation and the Henderson equation gave identical estimates for the potential with scenario 1. The approximated equation, which uses average conductivity, differs just a tiny bit in the last decimals. When the concentration difference, Δc, increases, the difference between the predictions of the approximated equation and the two other equations increases.

For scenario 4, the Goldman equation and Henderson equation gave similar estimates, while the approximated equation gave about two times larger estimates. Comparing scenario 4 to scenario 1, the calculated values with

scenario 4 is around double. An extended version of Table 4.2 can be found in Appendix A (on page 65), where I also included scenario 2 and scenario 3.

The Henderson and Goldman equations give almost identical estimates. Looking at the formulas, I see that the first fraction in the Henderson equation equals 1 when only K^+, Na^+, and Cl^- are used (the nominator will always be equal the denominator: $|z_i|/z_i = \pm 1$ when all have $|z_i| = 1$). This fraction can vary from 1 when we include other ion species with, for example, $|z_i| = 2$ (the denominator will then have a term with $|z_i| = 2$ and the nominator will have $|z_i|/z_i = \pm 1$). How much the fraction will vary from 1 depends on the concentration difference $(c_{i,2} - c_{i,1})$. If this concentration difference is small, the fraction will approximately equal 1. The two equations give same values for scenario 1 since the `ln()`-term become identical when $\Delta[Cl^-] = 0$. For scenario 4, the estimates from the two equations differ some, but overall both equations gave similar values.

I chose to use the Henderson equation when estimating the diffusion potential because it is better over distance (thick membranes [9]). I decided to only look at the absolute values when calculating the diffusion potential. This choice does not affect the calculation of PSDs.

4.3 Diffusion potentials for "normal" concentration data

The initial value of the diffusion potentials (Φ_0) is calculated using the concentration data in Table 4.1 (on page 36) and scenario 1 (see Section 3.3). I let the potential decay ($\Phi(t) = \Phi_0 \cdot e^{-t/\tau}$) for 100 s with the specified time constant from Table 4.1. For data without a specified time constant, I chose to use $\tau = 6$ s because it was the median of the other time constant.

Figure 4.1 (on page 39) shows how the estimated diffusion potentials decay exponentially over time. The largest initial diffusion potential is Hay-Yasein Fig 2b starting at ~ 0.30 mV. Most of the data get initial potentials between 0.1 and 0.25 mV, while four of the data (Cordingley Fig 5, Frölich2008 Fig 1B, Octeau Fig 1G, and Amzica Fig 3A) start at < 0.07 mV. All curves in Figure 4.1 seem to decay to a potential of 0.0 mV within the time interval of 100 s. As expected, the curves with the highest time constant decay slowest.
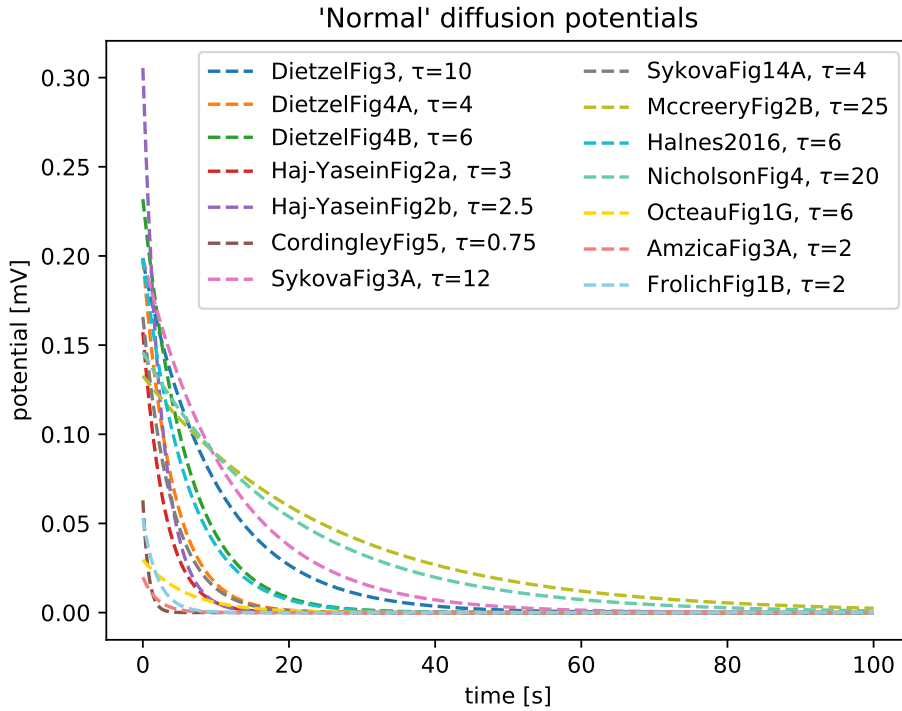
Figure 4.1: Exponentially decaying diffusion potentials for "normal" concentration data. The initial value of the diffusion potentials is estimated with the Henderson equation. The time constant for each curve is shown in the legend of the figure. The decay of the potentials is estimated for 100 s.

4.4 PSDs of "normal" diffusion potentials

For the exponentially decaying diffusion potentials in Figure 4.1, I calculated the PSDs as specified in Chapter 3 (see Section 3.6). The PSDs are shown in Figure 4.2 (on page 40) on a log-log plot.

The PSD lines in Figure 4.2 with time constants < 10 s have deflection for lower frequencies (a smaller slope between -2.0 to -1.0). At -1.0 the Haj-Yasein Fig 2b (purple) has the highest power, and Dietzel Fig 4B (green) has the next highest power. Most of the lines are located in this upper group. The same four lines (Cordingley Fig 5, Octeau Fig 1G, Amzica Fig 3A, Frölich2008 Fig 1B) with the lowest initial potential have the lowest powers, and they form the lower group.

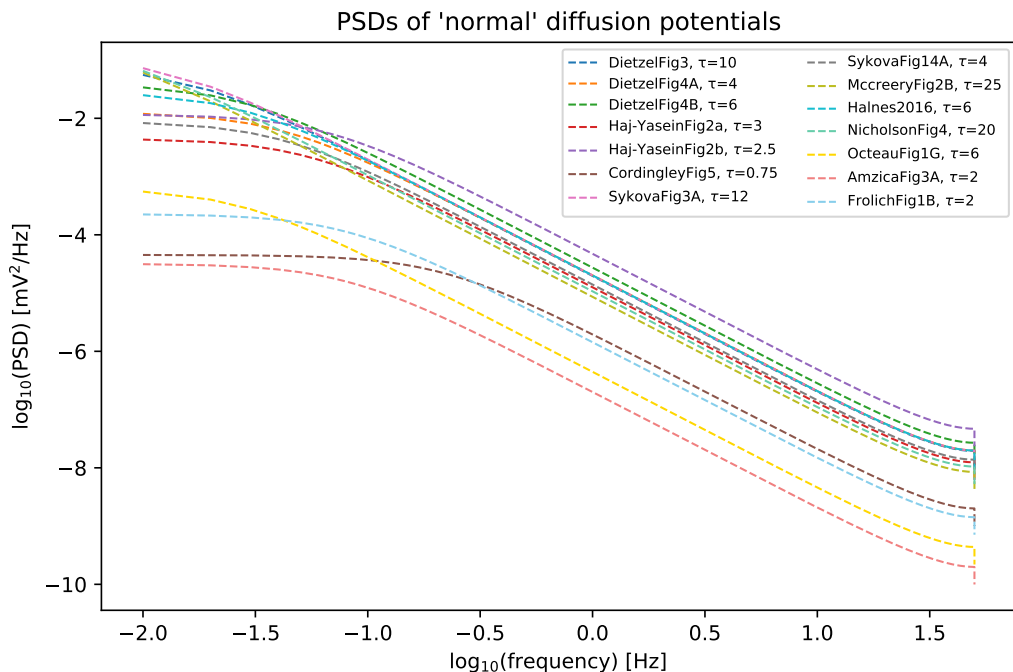All lines seem to follow a $1/f^2$ power law between between -0.5 and 1.5 ($\sim$0.3 and 32 Hz)

Figure 4.2: Power spectrum densities (PSDs) of the exponentially decaying diffusion potentials on a log-log plot. Smaller time constants give a deflection for the lowest frequencies.

4.5 PSDs of LFP data

4.5.1 PSDs of LFP data from articles

In this section, I present the PSD of LFPs found from three figures and two LFP data files. They are listed in Table 4.3 (on page 41) with some information, along with a short description and the assumptions made. The data are from different experiment in different animals and brain regions. The PSDs are shown in Figure 4.3 (on page 42).

Baranauskas et al. [30] recorded LFP in the somatosensory cortex of rats within the frequency range of 0.025 and 250 Hz. The data is spectral power density of an LFP signal with a frequency range of 0.1-100 Hz. Above ~1 Hz, the PSD follows a $1/f^{2.06}$ power law [30].

Jankowski et al. [31] recorded LFP from the anterior claustrum of rats. The data are mean PSD of LFP recordings from sessions in an environment in darkness, with a frequency range of 0-40 Hz [31].

Miller et al. [32] recorded electrocorticographic (ECoG) potentials with

40

Table 4.3: Overview of PSD of LFP data from three figures and two LFP data files. The paper and original figure is stated, along with a short description and assumptions made.

Taken from	Figure/Data	Description/Assumptions
Baranauskas et al. [30]	Figure 1C	somatosensory cortex of rats, assumed log-log axes with max y value equal 10^5 μV^2/Hz (not the originally 10^4)
Jankowski et al. [31]	Figure 2F	anterior claustrum of rats, mean PSD of LFP recordings, not log-log axis.
Miller et al. [32]	Figure 2A	averaged PSD over all channels in subject 1 for ECoG recordings, frequency range from ∼10 Hz to ∼1000 Hz, log-log axes
Torbjørn V. Ness[a]	data file	calculated averaged PSD of LFP recordings in mice Cut-off frequency was 0.1 Hz.
Gratiy et al. [24]	data file [33]	calculated mean PSD of LFP recording in mice

[a]unpublished data from Torbjørn V. Ness, obtained during the project [34]

electrodes placed on the subdural part of the human cortex. The human subjects had epilepsy and were implanted with electrodes to locate seizure focus. The data were recorded at the bedside during a fixation task, and the PSDs were averaged [32]. They fitted a power law, $1/f^\chi$, where they found that $\chi = -4$ for a frequency range of 80 to 200 Hz. They also applied a power law for frequencies between 15 and 80 Hz and got $\chi = -2.5$.

Torbjørn V. Ness provided me with a data file containing LFP recordings over 13 channels. The data is unpublished, but was obtained during a project by Thunemann et al. [34]. The recordings were done in a mouse with current stimuli applied to its whiskers. I calculated a mean PSD, which can be seen in Figure 4.3 (on page 42).

Gratiy et al. [24] used *in vivo* recordings of the extracellular potential (LFP) from the primary visual cortex of mice. The mice were exposed to visual stimuli, different light intensities, from a light source switching on and off [24]. I calculated the mean PSD from the LFP recordings, and it is shown in Figure 4.3.
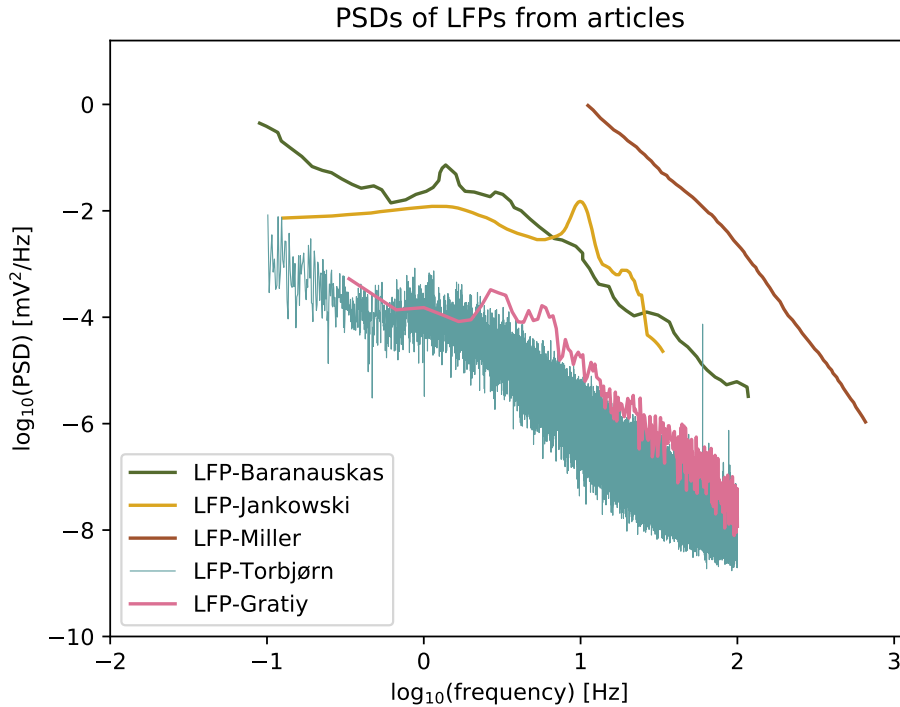
Figure 4.3: PSD of LFP recordings found from three figures (Baranauskas, Jankowski, and Miller) and PSD calculated from two LFP data files (Torbjørn and Gratiy). Baranauskas and Jankowski are from LFP recorded in rats, and Miller is ECoG from human cortex. The data from Torbjørn V. Ness and Gratiy et al. are LFP recorded in mice. For LFP-Torbjørn, I omitted the PSD for frequencies lower than 0.1 Hz and higher than 100 Hz. For LFP-Gratiy, I omitted the PSD for frequencies over 100 Hz. See Table 4.3 for more information.

4.5.2 PSDs of LFP recordings from CRCNS data sets

The data sets containing LFP recordings from the CRCNS data sharing site are summarized in Table 4.4[1]. Additional information, such as the specific data files and the sampling rates, can be found in Appendix B (on page 67).

The PSDs of the LFP recordings from the CRCNS data files are shown in Figure 4.4. The PSDs are averaged over all the recording channels and calculated as described in Section 3.6 and Section 3.7. In each data sets, there exist recordings from different sessions, conditions, and subjects. The abbreviations A, B, C, and D distinguish between the data files used and are specified in Table B.1 (see Appendix B).

---

[1]More information about the data sets can be found on the 'about' page for each data set and/or in the corresponding articles cited.

Table 4.4: Overview over the CRCNS data sets with LFP recordings I used.

| Dataset	Brain region	Description
hc-2 [35, 36]	hippocampus (layer CA1)	Multichannel recordings from three Long-Evans rats, under open field tasks. LFPs was extracted from the processed raw (broadband) data.
ac-2 [37]	auditory cortex	Recordings in response to pure tones with different amplitude and frequency, and nearby LFP recordings in rats.
pfc-2 [38, 39]	prefrontal cortex (and CA1 of hippocampus)	Recording of multi single neuron in three rats during memory task. Simultaneously monitored in pfc and CA1 of hippocampus.
bf-1 [40, 41]	basal forebrain	LFP recordings from rats (wild type *rattus norvegicus*) obtained under (i) resting condition (in home cage) and (ii) exploration of an arena
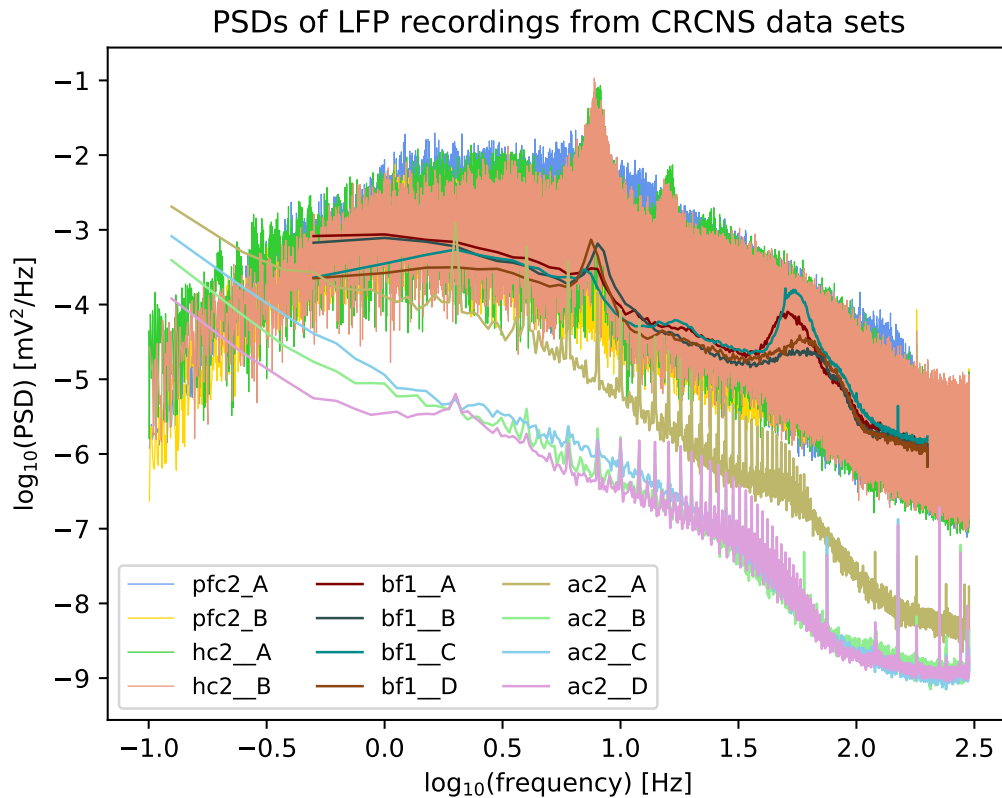
Figure 4.4: PSDs of LFP recordings from CRCNS data sets (see Table 4.4)

The PSDs from hc-2 (hippocampus) and pfc-2 (prefrontal cortex) overlap each other. The deflection of these between -1.0 and 0.0 (0.1 and 1.0Hz) is most likely because of a cut-off frequency on the recording electrode. Therefore, we can not fully trust these data sets in this frequency range. All the curves from the bf-1 (basal forebrain) data set are close together. The bf-1 curves also appear within the powers of both the hc-2 and pfc-2 data sets. The three lowest ac-2 (auditory cortex) curves lie on top of each other, and the fourth line (ac-2-D) has slightly higher powers. It seems that these ac-2 curves still increase for lower frequencies, unlike the hc-2 and pfc-2.

4.5.3 Selecting the PSDs to use in comparison

In Figure 4.5 I included the PSDs of LFP data from Figure 4.3 and Figure 4.4. The PSDs I used to compare with the PSDs of diffusion potentials are LFP-torbjørn, LFP-Gratiy, LFP-Baranauskas, bf-1-A, ac-2-A, and ac-2-D. These are shown with color in Figure 4.5. I chose these as a representative selection of all the PSDs of LFP data collected.

I chose the bf-1-A curve because it overlaps the PSDs of hc-2 and pfc-2 data for most of the frequency range. The ac-2 curves have a good frequency range, and I chose the highest and lowest PSDs. I selected the LFP-Baranauskas because it has the highest power for the low frequencies. I kept LFP-Torbjørn and LFP-Gratiy because of their low and medium PSD powers.
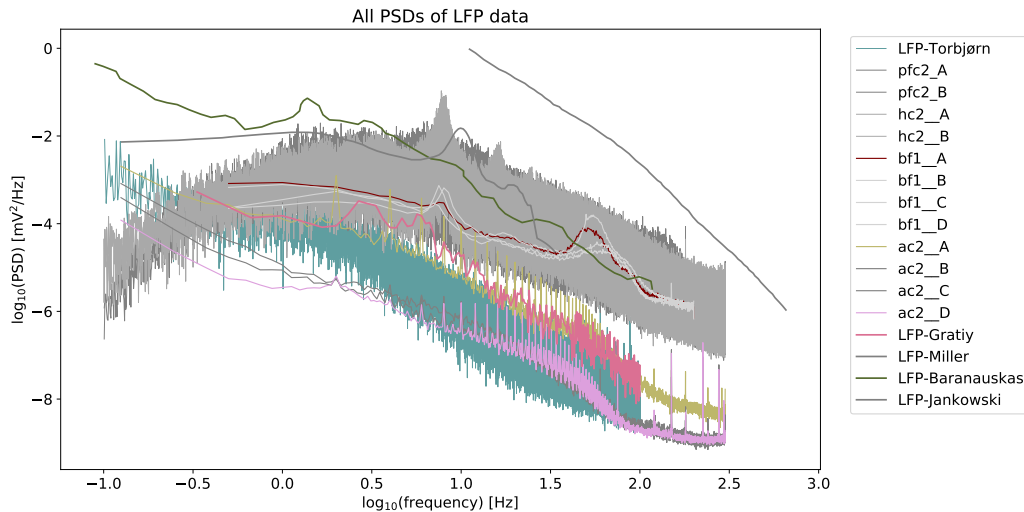

Figure 4.5: All PSDs from LFP data. The colored curves will be used further.

4.6 PSDs of LFPs versus PSDs of "normal" diffusion potentials

Figure 4.6 shows the PSDs of the "normal" diffusion potentials from Figure 4.2 together with the chosen PSDs of LFP recordings (the colored curves in Figure 4.5). For more readability of Figure 4.6, I included a zoomed-in verison (see Figure 4.7). A complete figure with all PSDs shown earlier is included in Appendix C (see Figure C.1 on page 71).
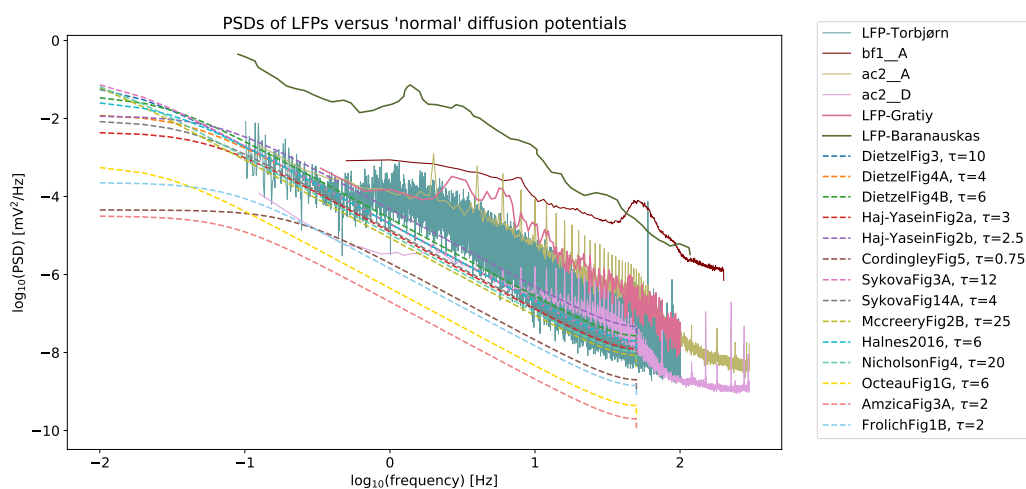

Figure 4.6: PSDs of the "normal" diffusion potentials and the chosen LFP recordings.
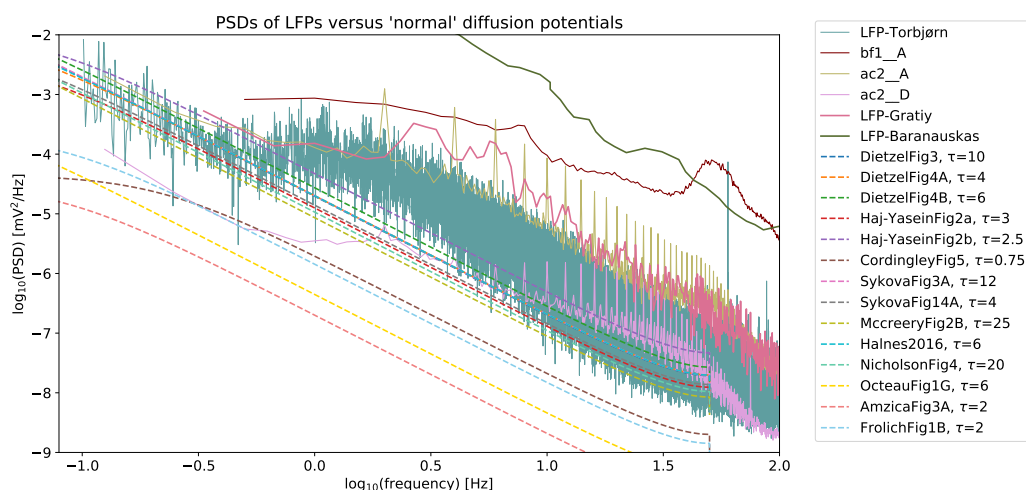

Figure 4.7: Zoomed-in version of Figure 4.6.

45

As seen from Figure 4.7 most of the PSDs of the "normal" diffusion potentials (in the following referred to as the PSD diffusion lines) have lower powers than the PSDs of LFP measurements. The LFP-Baranauskas, LFP-Gratiy, and bf1-A do not cross the PSD diffusion lines at any frequency. All the PSDs of LFP recordings have a cut-off frequency. Saying something about what happens below such a cut-off frequency is just speculation because we are outside the original frequency range. Even so, both LFP-Baranauskas and LFP-Gratiy seem to increase to higher powers for frequencies below their cut-off frequency. If so, they would also have higher power than the PSD diffusion lines for the lower frequencies. Looking at the bf1-A curve, there does not seem to be a similar increase for frequencies below its cut-off frequency. This curve could, therefore, possibly intersect some of the PSD diffusion lines at lower frequencies. However, this is just speculation, and I observed no intersection points within the frequency range of the bf-1-A curve.

The upper group of PSD diffusion lines consists of (listed in order from highest to lowest power): (1) Haj-YaseinFig2b, (2) DietzelFig4B, (3) SykovaFig3A, DietzelFig3, Halnes2016, and DietzelFig4A (overlapping lines), (4) SykovaFig14A, (5) Haj-YaseinFig2a, (6) NicholsonFig4, and (7) MccreeryFig2B. All these lines have Δc between +4 mM and +9.25 mM for extracellular K^+ (see Table 4.1), which can be considered rather large. In these cases, Δc amounts to about a doubling or tripling of the baseline K^+ concentration in the ECS.

All the lines in the upper group overlap with the PSD labeled LFP-Torbjørn between -1.0 and -0.3. (0.1 and $\sim$0.5 Hz). The PSD diffusion line with the highest power, Haj-YaseinFig2b, is the only one to intersect with the ac-2-A at a log-frequency around -0.4 ($\sim$0.4 Hz).

Most interesting is the point of intersection with the ac-2-D curve. All the PSD diffusion lines in the upper group have higher power than the ac-2-D curve for log-frequencies lower than 0.25 ($<$1.8 Hz). Some of the PSD diffusion lines (those with the highest power: (1), (2), and (3)) in Figure 4.7 have higher power than the ac-2-D curve, also between log-frequencies of 0.25 and $\sim$1.0 (1.8 and 10 Hz).

The lower group of PSD diffusion lines consist of: (8) CordingleyFig5, (9) FrolichFig1B, (10) OcteayFig1G, and (11) AmzicaFig3 (in order from highest to lowest power). All these lines have Δc between +0.5 and +1.89 for extracellular K^+ (see Table 4.1). Therefore, the lower group might be

46

more likely to represent PSDs for diffusion potentials for the most normal concentration differences. The two upper PSD diffusion lines in the lower group, (8) and (9), intersect with the ac-2-D curve between log-frequencies of -0.5 and -0.25 (0.3 and 0.6 Hz).

Both ac-2 curves in Figure 4.6 seem to follow a similar trend as the PSD diffusion lines for the lowest frequencies. There seem to be a lot going on in the auditory cortex at log-frequencies of 1.0 and 2.0 (10 and 100 Hz). Following the ac-2 curves toward the left, it appears to decline at around 0.5 ($\sim$3 Hz) before it again increases, approaching even lower frequencies. The shape of the ac-2 curves at these low frequencies seems to have similar shape as the PSD diffusion lines, which may indicate that a diffusion potential could have dominated the LFP recordings here.

In Figure 4.6 and Figure 4.7, it seems that only the highest PSD diffusion lines intersect and/or overlap with the lowest of the PSDs from LFP recordings. This means that for cases with relatively large concentration differences in ECS (but not pathological), the PSDs of diffusion potentials have the same magnitude as PSD of measured LFP for low frequencies. If it exits such concentration gradients in the LFP data with low power, these could possibly have great impact on the measured data. Thus, diffusion potential may influence LFP recordings.

4.7   PSDs for LFPs versus PSDs of "pathological" diffusion potentials

The concentration data collected for "pathological" cases are shown in Table 4.5 (on page 48). The table structure is similar to Table 4.1. Most of the data is for the case of spreading depression (SD), but I have also included some seizure data in the table. The type of data is specified in the 'Note' column of Table 4.5.

4.7.1   Diffusion potentials for "pathological" concentration data

The initial value of the "pathological" diffusion potentials, Φ_0, is calculated with the Henderson equation. The concentration data from Table 4.5 and scenario 4 are used to find the concentrations of the unmeasured ion species.

Table 4.5: "Pathological" concentration data (spreading depression and seizures). The table shows where data is taken from, the extracellular concentration of an ion (with baseline and maximum difference Δc), and the corresponding time constant for the ionic concentration decay. Some additional information about the data is provided under the 'Note' column.

Taken from	Concentrations (ion, base, Δc) [mM]	Time constant, τ_{decay} [s]	Note
Enger Fig 4F [42]	K^+, 3, +19	$t_{rise} \approx 22$s	cortical SD in
Enger Fig 4G [42]	K^+, 3, +23	$t_{rise} \approx 15$s	visual cortex of
Enger Fig 4H [42]	K^+, 3, +28	$t_{rise} \approx 14$s	adult living mice
Herreras Fig 1 [13]	K^+, 3, +51	$\sim$30s	SD, CA1 strata, in rats
Sykova Fig 14B [25]	K^+, 4, +28	$\sim$18s	evoked SD by strong simulation, rat cerebellum
Sykova Fig 24 [25]	K^+, 2, +38	$\sim$130s	SD, catfish cerebellum
Hansen Fig 1 [15]	K^+, 3, +50	$\sim$16s	cortical SD, recorded in parietal cortex, rats
Hansen Fig 2 [15]	K^+, 3, +47	$t_{rise} \approx 12$s	initial cortical SD, rat cortex
Kraig Fig 4 [14]	K^+, 2.3, +36	$\sim$125s	SD, catfish
Nicholson Fig 3 [43]	K^+, 3, +33	$\sim$20s	SD, rat cerebellar cortex
Amzica Fig 6B [28]	K^+, 3, +8	-	spike-wave seizures, cerebral cortex of cats, max to baseline: $\sim$13s
Amzica Fig 7 [28]	K^+, 3, +3.5	- (no time axis)	spike-wave seizures, suprasylvian gyrus, cats
Fröhlich Fig 1C [29]	K^+, 3, +7	-	Tonic-Clonic Seizure, after clonic phase $\sim$ 2.5s decay, in cat pericruciate cortex
Dufour Fig 5 [44]	K^+, 3, +4	$\sim$14s	during epileptic seizures, in cortex of adult cats
Raimondo Fig 1[45]	K^+, 4, +7	- (no time axis)	during seizure, only representative changes

As earlier, I let the initial diffusion potentials decay for 100 s with time constants from Table 4.5. For the cases with no time constant in Table 4.5, I assumed a time constant of 20 s because it was around the median for the other time constants.

Figure 4.8 shows the exponentially decaying diffusion potentials for the "pathological" concentration data. The largest initial diffusion potential is Herreras Fig 1, with a value of ∼4.0 mV. Hansen Fig 1 and Hansen Fig 2 also have initial values around 4.0 mV. The middle group has initial values between 1.0 and 3.0 mV. The smallest initial values are for the seizure cases, which have values below 1.0 mV. Most of the diffusion potentials in Figure 4.8 decay to a potential of 0.0 mV within the 100 s. Three of the curves (Herreras Fig 1, Kraig Fig 4, and Sykova Fig 24) do not reach 0.0 mV within the time interval of 100 s.
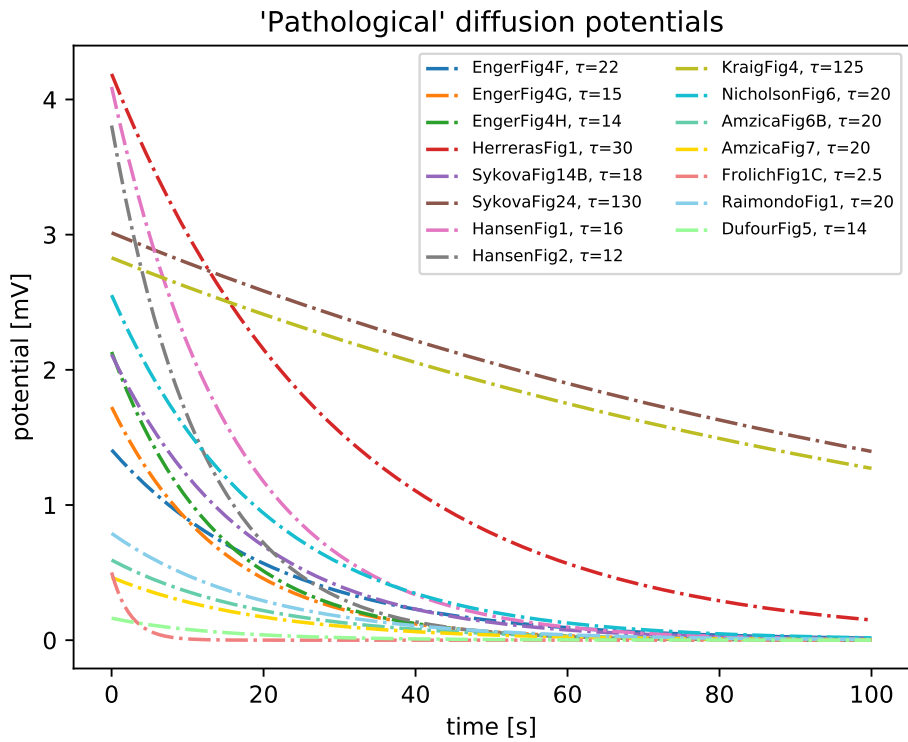

Figure 4.8: Exponentially decaying diffusion potentials for the "pathological" concentration data. The initial value of the diffusion potentials is estimated with the Henderson equation. The time constant for each curve is shown in the legend of the figure. The decay of the potentials is estimated for 100 s.

4.7.2 PSDs of "pathological" diffusion potentials

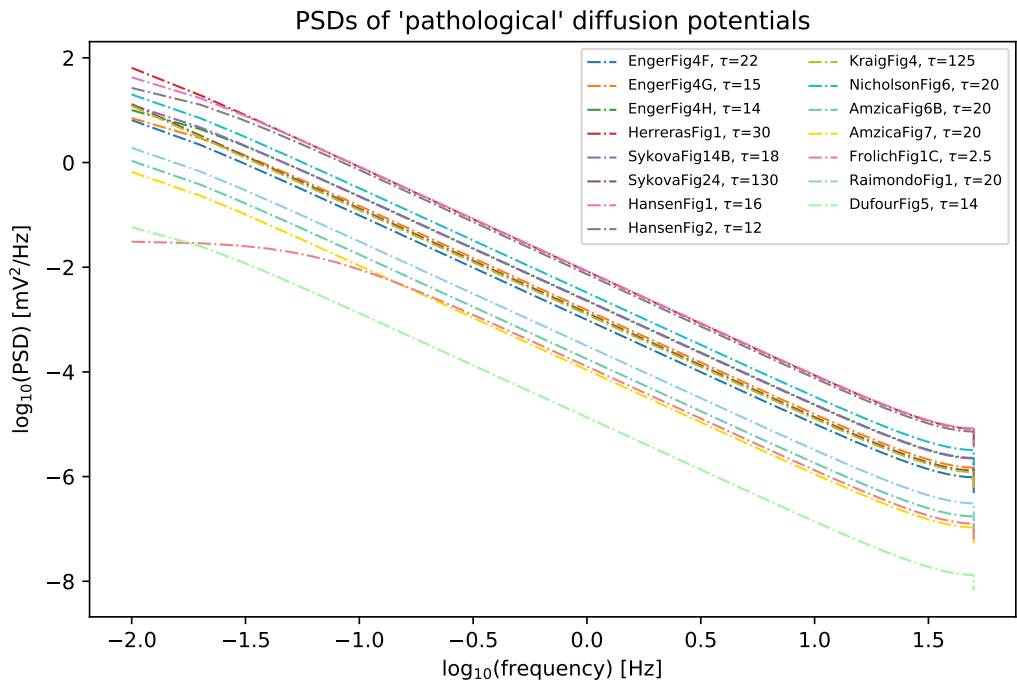The PSDs of the exponentially decaying diffusion potentials in Figure 4.8 are shown in Figure 4.9.

Figure 4.9: Power spectrum densities (PSDs) of the exponentially decaying diffusion potentials for the "pathological" concentration data. The axis is log-log. The five lowest PSDs are the seizure cases, while the others are the spreading depression (SD) cases.

As seen in Table 4.5 the time constants for K^+ decay in ECS during spreading depression range from 16s to 130s. I consider this as a wide range for time constants, and many scenarios of SD are therefore covered in the estimated PSDs. For most of the seizure cases, I did not find corresponding time constants and used an assumed value of 20 s (around the median of the other time constants). The same range in time constants are therefore not apparent for the seizure data.

4.7.3 PSDs of LFPs versus PSDs of "pathological" diffusion potentials

To compare PSDs of "pathological" diffusion potentials, I present similar figures as those in Section 4.6. Figure 4.10 shows the PSDs of "pathological" diffusion potentials from Figure 4.9 together with the chosen PSDs of LFP recordings (the colored curves in Figure 4.5). For more readability of Figure 4.10, I included a zoomed in verison (see Figure 4.11). A complete figure including all PSDs from LFP data are shown in Appendix C (see Figure C.2 on page 72).
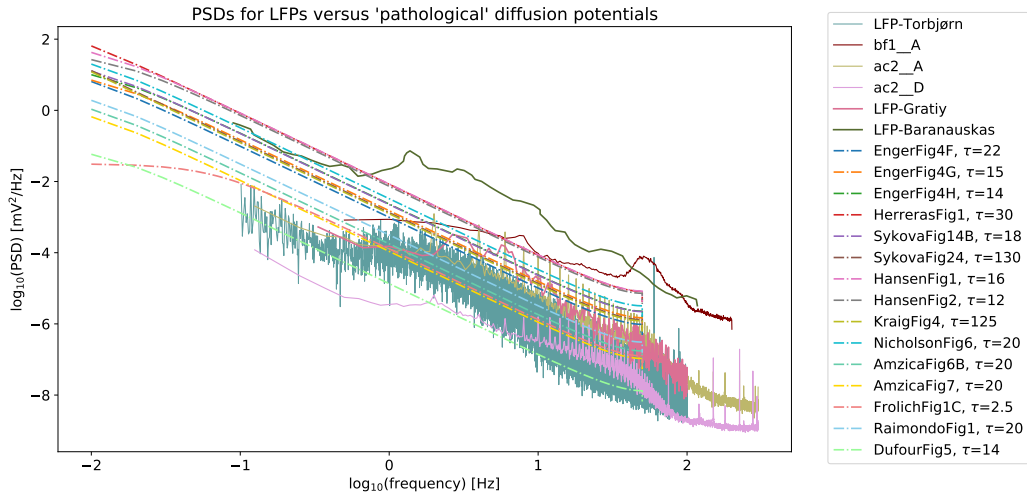

Figure 4.10: PSDs of the "pathological" diffusion potentials and the chosen LFP recordings.

As seen in Figure 4.11 (on page 52), all the PSDs of the "pathological" diffusion potentials (except the lowest one, DufourFig5) have higher power than the PSD diffusion lines in Figure 4.7. The concentration change of extracellular K^+ is substantial under SD, which leads to larger diffusion potentials and larger powers of their PSDs (the upper ten PSD lines). In the following, I will refer to the PSDs of the "pathological" diffusion potentials as the PSD pat-lines.

The five lowest PSD pat-lines are the seizure data (see the five lowest rows in the Table 4.5). Worth mentioning here is that the concentration differences in K^+ are within the same range as the concentration differences for the upper group in Figure 4.7. The only difference when calculating the diffusion potential is the scenario used for finding the unmeasured species
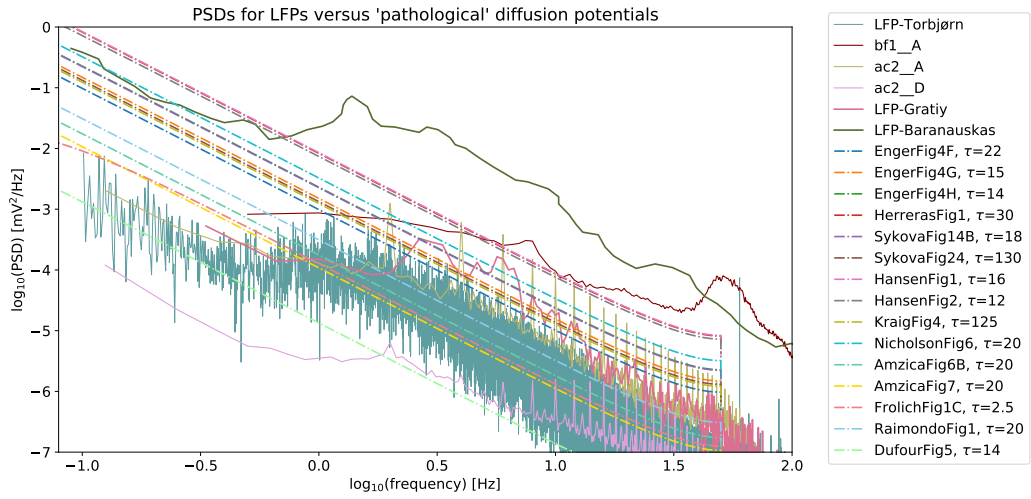
Figure 4.11: Zoomed-in version of Figure 4.10

(scenario 1 vs. scenario 4). Scenario 4 gave a higher absolute value for the diffusion potential and therefore also slightly higher powers for the PSD. With that said, four of these lines intersect LFP-Gratiy, LFP-Torbjørn, ac-2-A at log-frequency around 0.0 (1.0 Hz). The same four lines have higher powers than ac-2-D for all frequencies. This resembles what we saw earlier for the upper group of PSD diffusion lines in Figure 4.7 (on page 45).

All PSDs for spreading depression cases (ten upper PSD pat-lines) have higher powers than LFP-Torbjørn and ac-2-D. The three upper lines intersect the LFP-Baranauskas curve at around -0.2 (∼0.6 Hz). The bf-1-A curve has crossing points with the PSD pat-lines between log-frequencies of 0.0 and 0.6 (1 and 4 Hz).

The intersection points of Figure 4.11 indicated that diffusion potentials calculated for "pathological" cases (with large concentration differences, Δc) possibly could dominate LFP recordings for most frequencies, especially for the low frequencies.

Chapter 5

Discussion and Conclusion

The comparison of PSDs in Figure 4.6 shows that the PSDs of diffusion potentials for "normal" concentration data, for the most part, have lower powers than the PSDs of LFP recordings. However, Figure 4.6 also indicates that diffusion potentials, in some cases, possibly can contribute to the LFP recordings for low frequencies.

My results indicate that people measuring LFP can not exclude diffusion effects entirely because they may impact the measurements. Thus, it is not 100 % certain that LFP only reflects what the neurons are doing at the time of recording.

For the "pathological" cases, Figure 4.11 shows that almost every PSD for diffusion potentials has higher power than most of the LFP recordings. The diffusion potential can therefore dominate LFP measurements for most frequencies.

5.1 Project assumptions

To estimate the time-varying diffusion potentials, I made several assumptions. I believe these to be the most reasonable regarding my project. In the subsections below, I discuss my assumptions.

5.1.1 The two-point system and temporal data

My simplification to use a two-point system is the primary assumption for the project. Reducing spatial concentration profiles to two points was easy and

practical when the purpose was to only look at the maximum concentration differences.

I assumed that I also could use this two-point system for temporal data. Then, I assumed that point A ("before"/baseline) exists in another point in the ECS simultaneously as point B (peak/maximum concentration difference) exists. That is, when the concentrations change locally to a peak value (point B), there are still baseline concentrations (point A) in another area of the brain. I estimated the diffusion potential between point A and point B.

Both examples in Figure 3.2 (on page 24) show that the maximum concentration difference (point B) and the baseline (point A) exist spatially separated at the same point in time, and thereby provides some support for this assumption. The two-point system also allowed for the collection of a wide range of concentration data.

5.1.2   Small errors in collection of concentration data

Most of the concentration data is collected by visual inspection of the figures in articles. Zooming in and measuring concentration bars and time bars might give some errors. The diffusion potential depends linearly on Δc. A small reading error of Δc will result in small errors for the estimated diffusion potential. Such errors will have relatively little impact on the PSD lines, which are rather insensitive to small reading errors. Therefore, these errors are assumed to be so small that they do not impact the overall conclusion.

5.1.3   The scenarios used for unmeasured ion species

For the calculations of the diffusion potential, I wanted to include K^+, Na^+, and Cl^-. Recording of ECS concentration often involves only one or two ion species. To utilize most concentration data, assumptions for the concentration of unmeasured ion species were necessary. The scenarios were proposed and compared by Videm [10]. When only one ion species is known, Videm found scenario 1 to be the best scenario. The comparison performed by Videm [10] was the reason I chose scenario 1.

Both scenario 2 and scenario 3 gave smaller absolute values for the diffusion potential calculated with the Goldman and Henderson equations, while scenario 4 (used for "pathological" cases) gave twice as large values (see Table A.1 on page 65).

Regarding the three equations, the approximated equation gave only similar values to the Goldman and Henderson equation for scenario 1. For the other scenarios, this equation gave much larger estimates for the diffusion potential than the Goldman and Henderson equations (see Appendix A).

Choosing scenario 2 or 3 for the "normal" cases, would give smaller powers for the PSD diffusion lines relative to what scenario 1 gave (see Appendix A). Regardless, I believe that choosing scenario 1 is best because of the comparison done by Videm [10]

5.1.4 Change of extracellular concentrations and corresponding time constants

For temporal data the time-varying K^+ concentration appears to have a rather exponential form between the peak value and the baseline (see Figure 3.2 and Figure 3.4). The rise of extracellular K^+ concentration can also resemble exponential growth. This makes it possible to find two time constants for most temporal concentration data: τ_{rise} and τ_{decay}. For most of the concentration data collected, I used the decay time constant. In some cases, it was not possible to find τ_{decay}, so I used the rise time constant instead.

Finding and using the time constant from concentration data is indeed an approximation. The concentration data would certainly not fit a perfect exponential. In regards to other mathematical functions, the concentration decay could maybe be estimated with, for example, the sigmoid function $1/(1 + e^{-t})$, a parabola, or just $1/ct$. In the early stage of the project, I tested such functions and found that the exponential function, $e^{-t/\tau}$, was the best fit.

Regarding the time constant, I also assumed that the estimated diffusion potential decay with the same time constant as the extracellular K^+ concentration. Considering that the diffusion potential is a direct and seemingly instant response to concentrations of ion species, I believe this assumption to make sense. Using the K^+ time constant, we indirectly assume that the unmeasured ion species approach baseline with the same time constant. This is not necessarily correct, but possibly the best assumption regarding the lack of simultaneously measured ion species.

Assuming scenario 1, where $\Delta[K^+] = -\Delta[Na^+]$ and $\Delta[Cl^-] = 0$ this has to be the case. Na^+ must change accordingly to K^+ such that the electroneutrality criterion is fulfilled. With all three ion species present, a reduction of

K$^+$ can be compensated by an increase in Na$^+$, a decrease in Cl$^-$ or a mix of both. With a mix of both, the ion species do not necessarily change with similar amounts and/or with similar time constants.

5.2 "Comparing apples and oranges"

The comparison between the PSDs of diffusion potentials and PSDs of LFP recordings in Chapter 4 can be associated with the saying "comparing apples and oranges". The expression claims that there is no means in comparing the two since they are two different things. Why not? Apples and oranges have many similarities. They are both considered to be fruits, they grow on trees, and they have similar size and shape. In addition, apples and oranges are edible and can be used to make delicious juice.

In this project, PSDs are compared even though they originally are obtained from separate experiments conducted in different animal species. I have not come across cases where both extracellular ionic concentrations and LFP were measured simultaneously. Comparing PSDs from various circumstances may therefore be the only option.

The "apples" of the project are the PSDs of the diffusion potentials, which are calculated from concentration data of some experiments. The "oranges" are the PSDs of LFP recordings from other experiments. So, can the concentration differences observed in the "apples" also be present in the "oranges"?

Most of the concentration data and LFP data in this project are collected from cats, rats, and mice. The data was recorded in different locations, such as the cortex, hippocampus, and spinal cord, to mention some. The LFP recordings used from the CRNCS data sets were all recorded in rats. Figure 4.4 (on page 43) shows that LFP recordings from the same animal can give somewhat different PSDs due to the brain regions and the conducted experiments.

LFP is measured relative to a reference electrode, which is placed "far away" from the recording site. The placement of this reference electrode can differ from experiment to experiment. For the estimated diffusion potentials, the reference point is the baseline concentrations in the ECS (point A). The reference electrode for LFP recordings and point A for the diffusion potentials should ideally be the same. I assumed this to be the case, so the PSD comparison makes sense, and I believe this assumption to be reasonable.

Another point concerning the PSD comparison, is that I can not validate how the PSDs obtained from figures were calculated. I have come across a few different formulas used for estimating PSDs. For this project, I investigated and validated the formula (see Section 2.5) used in SciPy's `periodogram` function for both the power spectrum (PS) and the power spectrum density (PSDs) (with the help of a forum[1]). Regarding the figures, I only used PSDs from figures with the same units as my calculated PSDs.

The diffusion potentials are calculated with the two-point system, between the baseline and the maximum concentration difference. Therefore, the estimated diffusion potentials can be seen as the maximal potential. For the "normal" cases, the PSDs of the maximal diffusion potentials only intersect or overlap with the lowest PSDs of LFP recordings. The question is then: could such concentration differences in the ECS exist during LFP recordings? Answering this question calls for a more thorough investigation.

5.3 Can diffusion potentials affect the extracellular potentials?

If LFP was measured during pathological cases, such as spreading depression, it is reasonable to think that the large concentration differences could affect the recordings. During more normal brain activity, similar concentration effects are uncertain. However, they should not be automatically excluded or neglected, as people normally do. Even though concentration gradients are slow-changing, they could have existed for a while before LFP measurements are taken and therefore also during the recording time.

For high frequencies, neglecting diffusion potentials is ok because they are slowly varying, and they will therefore not influence the ECS potential at these frequencies. For low frequencies, my results show that diffusion potentials possibly can be large enough to affect ECS potentials.

For non-pathological cases, the diffusion potentials have higher power than one of the LFP recordings for frequencies < 1 Hz. Most of the PSD of the "normal" diffusion potentials overlap another PSD of LFP recordings for frequencies between 0.1 and 0.5 Hz. For pathological cases involving large concentration gradients, the diffusion potentials have, not surprisingly,

---

[1]The forum is avaiable at: `https://stackoverflow.com/questions/22338415/scipy-periodogram-terminology-confusion` (Accessed: 21 April 2021)

higher powers than most of the LFP recordings for most frequencies. Such concentration differences can therefore affect LFP recordings.

The intersection points found in Chapter 4 can motivate further research of diffusion potentials and their effects on the extracellular potential. Moreover, it may also inspire to record both the diffusion potential and LFP or record LFPs with lower cut-off frequencies.

Chapter 6

Bibliography

[1] G. Halnes, T. Mäki-Marttunen, D. Keller, K. H. Pettersen, O. A. Andreassen, and G. T. Einevoll, "Effect of ionic diffusion on extracellular potentials in neural tissue," *PLoS computational biology*, vol. 12, no. 11, p. e1005193, 2016.

[2] D. Purves, G. J. Augustine, D. Fitzpatrick, W. C. Hall, A.-S. Lamantia, J. O. Mcnamara, and S. M. Williams, *Neuroscience*. Sunderland (MA): Sinauer Associates, 3rd ed., 2004.

[3] E. Syková and C. Nicholson, "Diffusion in brain extracellular space," *Physiological reviews*, vol. 88, no. 4, pp. 1277–1340, 2008.

[4] H. Kager, W. J. Wadman, and G. G. Somjen, "Simulated seizures and spreading depression in a neuron model incorporating interstitial space and ion concentrations," *Journal of Neurophysiology*, vol. 84, no. 1, pp. 495–512, 2000. PMID: 10899222.

[5] A. Solbrå, A. W. Bergersen, J. Van Den Brink, A. Malthe-Sørenssen, G. T. Einevoll, and G. Halnes, "A kirchhoff-nernst-planck framework for modeling large scale extracellular electrodiffusion surrounding morphologically detailed neurons," *PLoS computational biology*, vol. 14, no. 10, p. e1006510, 2018.

[6] G. G. Somjen, *Ions in the brain: normal function, seizures, and stroke*. Oxford University Press, 2004.

[7] D. Sterratt, B. Graham, A. Gillies, and D. Willshaw, *Principles of computational modelling in neuroscience*. Cambridge University Press, 2011.

[8] J. Strutwolf, G. Herzog, A. Homsy, A. Berduque, C. J. Collins, and D. W. Arrigan, "Potentiometric characterisation of a dual-stream electrochemical microfluidic device," *Microfluidics and nanofluidics*, vol. 6, no. 2, p. 231, 2009.

[9] J. W. Perram and P. J. Stiles, "On the nature of liquid junction and membrane potentials," *Physical Chemistry Chemical Physics*, vol. 8, no. 36, pp. 4200–4213, 2006.

[10] S. Videm, "Exploring the electric diffusion potential in the extracellular space of the brain," Master's thesis, Norwegian University of Life Sciences, Ås, 2018.

[11] I. Dietzel, U. Heinemann, G. Hofmeier, and H. Lux, "Stimulus-induced changes in extracellular na+ and cl- concentration in relation to changes in the size of the extracellular space," *Experimental brain research*, vol. 46, no. 1, pp. 73–84, 1982.

[12] C. Ayata and M. Lauritzen, "Spreading depression, spreading depolarizations, and the cerebral vasculature," *Physiological reviews*, vol. 95, no. 3, pp. 953–993, 2015.

[13] O. Herreras and J. Makarova, "Mechanisms of the negative potential associated with leão's spreading depolarization: A history of brain electrogenesis," *Journal of Cerebral Blood Flow & Metabolism*, vol. 40, no. 10, pp. 1934–1952, 2020.

[14] R. Kraig and C. Nicholson, "Extracellular ionic variations during spreading depression," *Neuroscience*, vol. 3, no. 11, pp. 1045–1059, 1978.

[15] A. J. Hansen and T. Zeuthen, "Extracellular ion concentrations during spreading depression and ischemia in the rat brain cortex," *Acta Physiologica Scandinavica*, vol. 113, no. 4, pp. 437–445, 1981.

[16] G. Cordingley and G. Somjen, "The clearing of excess potassium from extracellular space in spinal cord and cerebral cortex," *Brain research*, vol. 151, no. 2, pp. 291–306, 1978.

[17] G. Buzsáki, C. A. Anastassiou, and C. Koch, "The origin of extracellular fields and currents—eeg, ecog, lfp and spikes," *Nature reviews neuroscience*, vol. 13, no. 6, pp. 407–420, 2012.

[18] J. A. Henrie and R. Shapley, "Lfp power spectra in v1 cortex: the graded effect of stimulus contrast," *Journal of neurophysiology*, vol. 94, no. 1, pp. 479–490, 2005.

[19] E. Kreyszig, *Advanced Engineering Mathematics 10th Edition, International Student Version*. Publisher John Wiley & Sons, Inc., 2011.

[20] *123.physics.ucdavis.edu*. National Instruments Inc., "Tutorial on measurement of power spectra (2013)." `http://123.physics.ucdavis.edu/week_2_files/tutorial_on_measurement_of_power_spectra.pdf`, (Accessed 13 April 2021).

[21] C. Nicholson, G. Ten Bruggencate, H. Stockle, and R. Steinberg, "Calcium and potassium changes in extracellular microenvironment of cat cerebellar cortex," *Journal of neurophysiology*, vol. 41, no. 4, pp. 1026–1039, 1978.

[22] N. N. Haj-Yasein, C. E. Bugge, V. Jensen, I. Østby, O. P. Ottersen, Ø. Hvalby, and E. A. Nagelhus, "Deletion of aquaporin-4 increases extracellular k+ concentration during synaptic stimulation in mouse hippocampus," *Brain Structure and Function*, vol. 220, no. 4, pp. 2469–2474, 2015.

[23] P. Welch, "The use of fast fourier transform for the estimation of power spectra: a method based on time averaging over short, modified periodograms," *IEEE Transactions on audio and electroacoustics*, vol. 15, no. 2, pp. 70–73, 1967.

[24] S. L. Gratiy, G. Halnes, D. Denman, M. J. Hawrylycz, C. Koch, G. T. Einevoll, and C. A. Anastassiou, "From maxwell's equations to the theory of current-source density analysis," *European Journal of Neuroscience*, vol. 45, no. 8, pp. 1013–1023, 2017.

[25] E. Syková, "Extracellular k+ accumulation in the central nervous system," *Progress in biophysics and molecular biology*, vol. 42, pp. 135–189, 1983.

[26] D. B. McCreery and W. F. Agnew, "Changes in extracellular potassium and calcium concentration and neural activity during prolonged electrical stimulation of the cat cerebral cortex at defined charge densities," *Experimental neurology*, vol. 79, no. 2, pp. 371–396, 1983.

[27] J. C. Octeau, M. R. Gangwani, S. L. Allam, D. Tran, S. Huang, T. M. Hoang-Trong, P. Golshani, T. H. Rumbell, J. R. Kozloski, and B. S. Khakh, "Transient, consequential increases in extracellular potassium ions accompany channelrhodopsin2 excitation," *Cell reports*, vol. 27, no. 8, pp. 2249–2261, 2019.

[28] F. Amzica, M. Massimini, and A. Manfridi, "Spatial buffering during slow and paroxysmal sleep oscillations in cortical networks of glial cells in vivo," *Journal of Neuroscience*, vol. 22, no. 3, pp. 1042–1053, 2002.

[29] F. Fröhlich, M. Bazhenov, V. Iragui-Madoz, and T. J. Sejnowski, "Potassium dynamics in the epileptic cortex: new insights on an old topic," *The Neuroscientist*, vol. 14, no. 5, pp. 422–433, 2008.

[30] G. Baranauskas, E. Maggiolini, A. Vato, G. Angotzi, A. Bonfanti, G. Zambra, A. Spinelli, and L. Fadiga, "Origins of 1/f2 scaling in the power spectrum of intracortical local field potential," *Journal of Neurophysiology*, vol. 107, no. 3, pp. 984–994, 2012.

[31] M. M. Jankowski, M. N. Islam, and S. M. O'Mara, "Dynamics of spontaneous local field potentials in the anterior claustrum of freely moving rats," *Brain research*, vol. 1677, pp. 101–117, 2017.

[32] K. J. Miller, L. B. Sorensen, J. G. Ojemann, and M. Den Nijs, "Power-law scaling in the brain surface electric potential," *PLoS Comput Biol*, vol. 5, no. 12, p. e1000609, 2009.

[33] S. Gratiy, "Trial averaged LFP/CSD for Figure 2," 1 2018. `https://figshare.com/articles/dataset/Trial_averaged_LFP_CSD_for_Figure_2/4780321` (Accessed: 3 February 2021).

[34] M. Thunemann, T. V. Ness, K. Kılıç, C. G. Ferri, S. Sakadzic, A. M. Dale, Y. Fainman, D. A. Boas, G. T. Einevoll, and A. Devor, "Does light propagate better along pyramidal apical dendrites in cerebral cortex?," in *Microscopy Histopathology and Analytics*, pp. JW3A–56, Optical Society of America, 2018.

[35] K. Mizuseki, A. Sirota, E. Pastalkova, and G. Buzsáki, "Multi-unit recordings from the rat hippocampus made during open field foraging.," 2009. `http://dx.doi.org/10.6080/K0Z60KZ9`.

[36] K. Mizuseki, A. Sirota, E. Pastalkova, and G. Buzsáki, "Theta oscillations provide temporal windows for local circuit computation in the entorhinal-hippocampal loop," *Neuron*, vol. 64, no. 2, pp. 267–280, 2009.

[37] M. R. Deweese and A. M. Zador, "Whole cell recordings from neurons in the primary auditory cortex of rat in response to pure tones of different frequency and amplitude, along with recordings of nearby local field potential (lfp).," 2011. CRCNS.org, `http://dx.doi.org/10.6080/K0G44N6R`.

[38] S. Fujisawa, A. Amarasingham, M. T. Harrison, A. Peyrache, and G. Buzsáki, "Simultaneous electrophysiological recordings of ensembles of isolated neurons in rat medial prefrontal cortex and intermediate ca1 area of the hippocampus during a working memory task.," 2015. CRCNS.org. `http://dx.doi.org/10.6080/K01V5BWK`.

[39] S. Fujisawa, A. Amarasingham, M. T. Harrison, and G. Buzsáki, "Behavior-dependent short-term assembly dynamics in the medial prefrontal cortex," *Nature neuroscience*, vol. 11, no. 7, p. 823, 2008.

[40] J. Nair, A.-L. Klaassen, J. Arato, A. L. Vyssotski, M. Harvey, and G. Rainer, "Basal forebrain lfp recordings in home cage and during arena exploration.," 2018. CRCNS.org, `http://dx.doi.org/10.6080/K0MK6B2Q`.

[41] J. Nair, A.-L. Klaassen, J. Arato, A. L. Vyssotski, M. Harvey, and G. Rainer, "Basal forebrain contributes to default mode network regulation," *Proceedings of the National Academy of Sciences*, vol. 115, no. 6, pp. 1352–1357, 2018.

[42] R. Enger, W. Tang, G. F. Vindedal, V. Jensen, P. Johannes Helm, R. Sprengel, L. L. Looger, and E. A. Nagelhus, "Dynamics of ionic shifts in cortical spreading depression," *Cerebral Cortex*, vol. 25, no. 11, pp. 4469–4476, 2015.

[43] C. Nicholson, "Measurement of extracellular ions in the brain," *Trends in neurosciences*, vol. 3, no. 9, pp. 216–218, 1980.

[44] S. Dufour, P. Dufour, O. Chever, R. Vallée, and F. Amzica, "In vivo simultaneous intra-and extracellular potassium recordings using a micro-

optrode," *Journal of neuroscience methods*, vol. 194, no. 2, pp. 206–217, 2011.

[45] J. V. Raimondo, R. J. Burman, A. A. Katz, and C. J. Akerman, "Ion dynamics during seizures," *Frontiers in cellular neuroscience*, vol. 9, p. 419, 2015.

Appendix A

Extended scenario-comparison

Table A.1 shows the estimated values for the three equations (Goldman, Henderson, and Approximated) for the different scenarios (1-4).

Table A.1: Comparing the equations and the scenarios (1-4)

Scenario 1

$\Delta[K^+]$ [mM]	+2	+4	+6	+9
Goldman, Φ_G [mV]	-0.06558200	-0.13100340	-0.19626497	-0.29385936
Henderson, Φ_H [mV]	-0.06558200	-0.13100340	-0.19626497	-0.29385936
Approx, $\Delta\Phi$ [mV]	0.06558197	0.13100314	0.19626409	0.29385640

Scenario 2

$\Delta[K^+]$ [mM]	+2	+4	+6	+9
Goldman, Φ_G [mV]	–0.02905245	-0.05784541	-0.08638237	-0.12871524
Henderson, Φ_H [mV]	-0.02905264	-0.05784693	-0.08638742	-0.12873194
Approx, $\Delta\Phi$ [mV]	0.23968268	0.47722446	0.71265391	1.06189868

Scenario 3

$\Delta[K^+]$ [mM]	+2	+4	+6	+9
Goldman, Φ_G [mV]	0.00723949	0.01436801	0.02138809	0.03172023
Henderson, Φ_H [mV]	0.00723963	0.01436801	0.02138809	0.03172023
Approx, $\Delta\Phi$ [mV]	0.412651018	0.818976607	1.21912110	1.80805334

Scenario 4

$\Delta[K^+]$ [mM]	+2	+4	+6	+9
Goldman, Φ_G [mV]	-0.13936351	-0.28022935	-0.42262393	-0.63914161
Henderson, Φ_H [mV]	-0.13936453	-0.28023761	-0.42265226	-0.63923961
Approx, $\Delta\Phi$ [mV]	-0.28606129	-0.57520233	-0.86747313	-1.31185968
$\Delta[K^+]$ [mM]	+20	+30	+40	+50
Goldman, Φ_G [mV]	-1.46455467	-2.26119219	-3.10641952	-4.00528695
Henderson, Φ_H [mV]	-1.4657353	-2.26554703	-3.11774928	-4.02968968
Approx, $\Delta\Phi$ [mV]	-3.00543842	-4.63862524	-6.36915928	-8.20601157

Looking at the estimated values from the Goldman and Henderson equations in Table A.1, I see that estimates with scenario 2 were around 40% of the estimates calculated with scenario 1. For scenario 3, the estimates were about 10% of the scenario 1 estimates, and for scenario 4, the estimates were around two times larger than scenario 1.

For all scenarios, the estimates from the Goldman and Henderson equations are very similar. The approximated equation gave only similar estimates for scenario 1. For the other scenarios, this equation gave quite different values for the potential. rather

For scenario 4, I also included estimates when Δc was $+20$, $+30$, $+40$, and $+50$ for K^+ (since I used this scenario for spreading depression). For these cases, the Goldman and Henderson estimates differ in the second and third decimal. The approximated equation gave about twice as large values.

For the scenarios, I also compared how their PSD estimates would differ. I estimated PSDs for $\Delta[K^+] = +4$ and used a time constant $\tau = 5$ s for the exponential decay. Figure A.1 shows the calculated PSD for each scenario. Scenario 4 had the highest PSD line, then comes scenario 1 and scenario 2. Scenario 3 had the lowest PSD line.
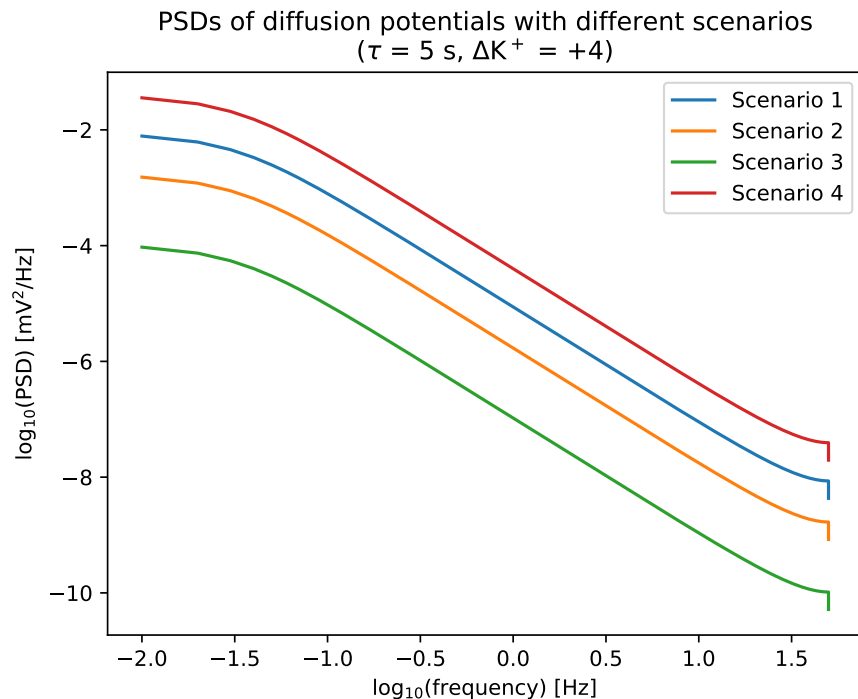

Figure A.1: PSDs for diffusion potential estimated with the Henderson equation and the different scenarios (1-4). The concentration difference for extracellular K^+ was $\Delta c = +4$ and the time constant of the the exponentially decay was $\tau = 5$ s.

Appendix B

LFP recordings

B.1 CRCNS data sets

Some more technical information for each CRCNS data set are given in Table B.1. The abbreviations used for each data file are also provided in the table.

Table B.1: Overview of the data files I used from the CRCNS data sets and some additional information such as file type and sampling rate.

Dataset	Data File	Note
hc-2 [35, 36]	ec013.527 (A) ec013.529 (B)	.eeg files (binary) contain LFP data (<625 Hz) sampling frequency = 1250 Hz data required a conversion factor to volt
ac-2 [37]	111500md01 (A) 030301md03b (B) 020901md01 (C) 020701md01b (D)	data stored in .mat files, data in mV sample rate = 4000 Hz some recordings required a correction factor unit of data is mV
pfc-2 [38, 39]	EE.042	.eeg file (binary) contain LFP data sample rate = 1250 Hz 64 channels in PFC (A), 32 channels in CA1 (B) data required a conversion factor to volt
bf-1 [40, 41]	Rat1Hcage1 (A) Rat1Arena1 (B) Rat3Hcage2 (C) Rat3Arena2 (D)	data stored in .mat files sample rate = 400 Hz assumed unit of LFP data to be in μV

The hc-2 data set [35] is used in Mizuseki et al. [36] where they studied theta bands (5-11 Hz). I found nothing about a possibly cut-off frequency for the data set. Though, in the supplementary information, they compare theta band frequencies to nearby bands (1-4Hz, 12-14Hz). With this information, I

decided to trust the data for frequencies > 1.0 Hz. The peak seen for the hc-2 lines in Figure 4.4 seems to appear at the theta band frequency (5-11 Hz is 0.70-1.04 in log10 scale). Since they studied the theta band, the stimuli used were probably meant to get responses in the theta band. I chose to cut the PSD data at 0.1 and 300 Hz when plotting (see Figure 4.4). The deflection between 0.1 and 1.0 Hz is most likely because of a cut-off frequency for the electrodes, so I do not fully trust the hc-2 data in this frequency range.

The LFP data in the pfc-2 data set [38] was not discussed in Fujisawa et al. [39] (the corresponding article). Anyhow, this data set had the same format as hc-2, and I could use MATLAB scripts provided with the hc-2 data set. In addition, the calculated PSDs from pfc-2 data had a similar shape as the PSDs from hc-2. Therefore, I used the same cutting of the PSDs calculated from pfc-2 data as used for hc-2 (plotted PSDs between 0.1 and 300 Hz). As with the hc-2 data set, I do not think the pfc-2 data in the frequency range between 0.1 and 1.0 Hz is fully trustworthy.

The ac-2 data set [37] is recorded in vivo with a whole-cell patch-clamp. It gave recordings of the membrane potential from neurons in the auditory cortex of rats. Each voltage trace in the data set has units of millivolts (mV) and is a response to a tone [37]. In addition, most recordings also contain simultaneously recorded local field potential (LFP). LFP was recorded with a second patch electrode about 1/2 mm from the whole-cell recording electrode [37]. I assume that the vertical lines appearing at higher frequencies are noise (see Figure 4.4). The PSDs from the ac-2 data set do not appear to deflect for lower frequencies, and I believe the PSDs to be reliable.

The bf-1 data set is used by Nair et al. [41]. They focused on gamma oscillations (>30 Hz), and one can see peaks in Figure 4.4 appearing for frequencies > 30 Hz. In the supporting information, they look into other low-frequency bands, in particular delta (1–5 Hz), theta (6–10 Hz), and beta (12–30 Hz). Peaks in the PSDs of bf-1 data also appear in the theta bands. I found no specification of the unit of the LFP data from bf-1. By comparing the PSDs I calculated, with the figures in Nair et al. [41], I assumed the units of LFP data to be in μV. In Nair et al. [41] they have figures showing spectral power for frequencies between 20-30Hz and 80 Hz. The supporting information shows spectral power for frequencies from $\sim$0-1 Hz to 80 Hz. Therefore, I do not cut the data but keep it as is.

B.2 Other data sets

Technical information for the data sets from Torbjørn V. Ness and Gratiy et al. [24] is given in Table B.2.

Table B.2: Technical information of data files with the LFP recordings from Torbjørn V. Ness and Gratiy et al. [24].

From	Information
Torbjørn[a]	`lfp_run26.npy` Sampling rate = 2000 Hz Cut-off frequency = 0.1 Hz.
Gratiy et al. [24, 33]	`mouse_1_lfp_trial_avg_3sec.h5` Sampling rate = 2500 Hz used "flash_off" LFP recodings

[a]unpublished data from Torbjørn V. Ness, obtained during the project [34]
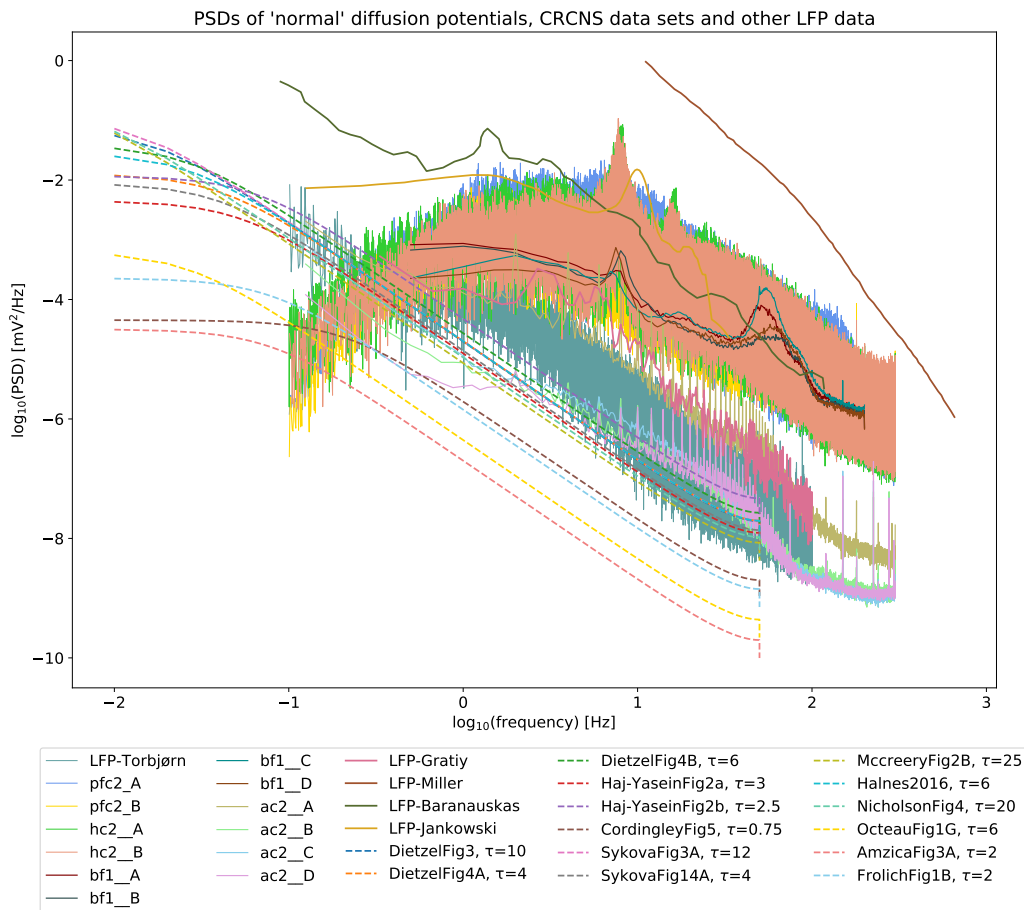
Appendix C

Extended figures

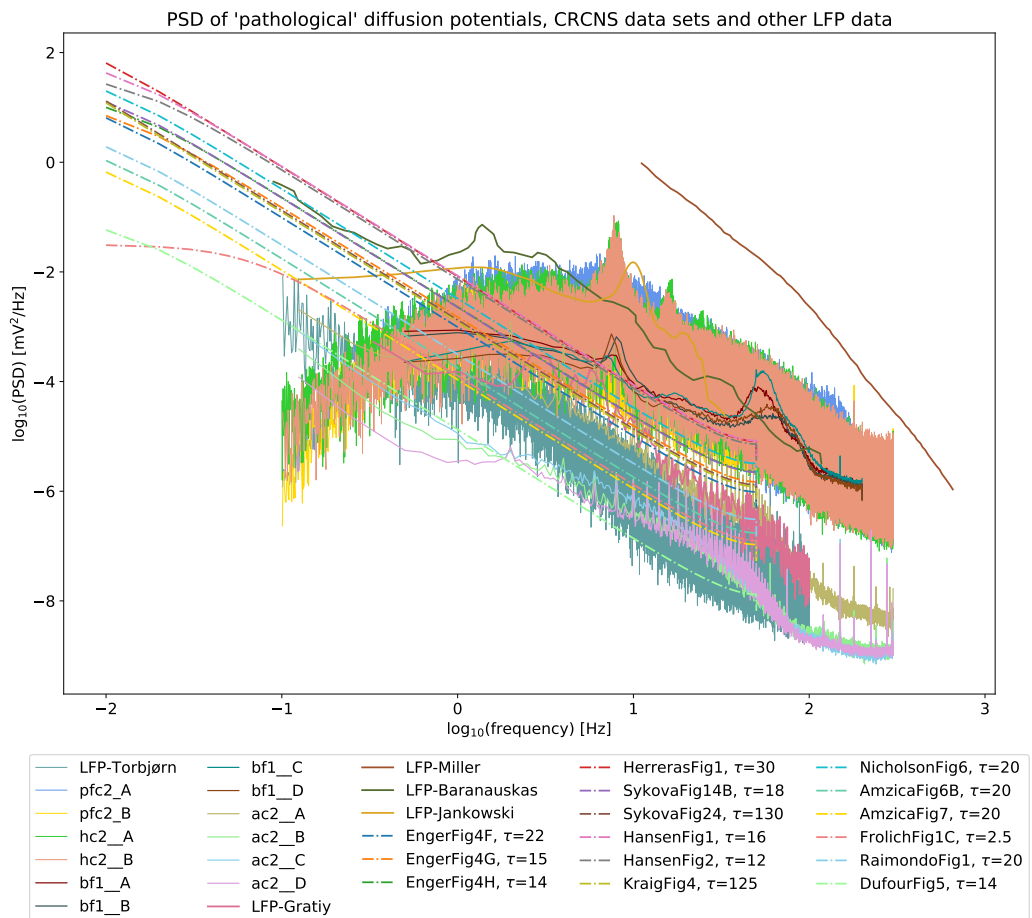**Figure C.1:** PSD of "normal" diffusion potentials, CRCNS data sets and other LFP data

Figure C.2: PSD of "pathological" diffusion potentials, CRCNS data sets and other LFP data